Development/Plasticity/Repair

POU6f1 Mediates Neuropeptide-Dependent Plasticity in the Adult Brain

Cynthia K. McClard,[1,2] Mikhail Y. Kochukov,[1] Isabella Herman,[2,3] Zhandong Liu,[4,5] Aiden Eblimit,[6] Yalda Moayedi,[7] Joshua Ortiz-Guzman,[3] Daniel Colchado,[8] Brandon Pekarek,[1] Sugi Panneerselvam,[8] Graeme Mardon,[1] and Benjamin R. Arenkiel[1,3,5,7]

[1]Department of Molecular and Human Genetics, [2]Medical Scientist Training Program, [3]Program in Developmental Biology, [4]Department of Pediatrics at Texas Children's Hospital, [5]Jan and Dan Duncan Neurological Research Institute at Texas Children's Hospital, [6]Human Genome Sequencing Center, Department of Molecular and Human Genetics, [7]Department of Neuroscience, Baylor College of Medicine, Houston, Texas 77030, and [8]Rice University, Houston, Texas 77005

The mouse olfactory bulb (OB) features continued, activity-dependent integration of adult-born neurons, providing a robust model with which to examine mechanisms of plasticity in the adult brain. We previously reported that local OB interneurons secrete the neuropeptide corticotropin-releasing hormone (CRH) in an activity-dependent manner onto adult-born granule neurons and that local CRH signaling promotes expression of synaptic machinery in the bulb. This effect is mediated via activation of the CRH receptor 1 (*CRHR1*), which is developmentally regulated during adult-born neuron maturation. CRHR1 is a G_S-protein-coupled receptor that activates CREB-dependent transcription in the presence of CRH. Therefore, we hypothesized that locally secreted CRH activates CRHR1 to initiate circuit plasticity programs. To identify such programs, we profiled gene expression changes associated with CRHR1 activity in adult-born neurons of the OB. Here, we show that CRHR1 activity influences expression of the brain-specific Homeobox-containing transcription factor POU Class 6 Homeobox 1 (*POU6f1*). To elucidate the contributions of *POU6f1* toward activity-dependent circuit remodeling, we targeted CRHR1$^+$ neurons in male and female mice for cell-type-specific manipulation of *POU6f1* expression. Whereas loss of *POU6f1* in CRHR1$^+$ neurons resulted in reduced dendritic complexity and decreased synaptic connectivity, overexpression of *POU6f1* in CRHR1$^+$ neurons promoted dendritic outgrowth and branching and influenced synaptic function. Together, these findings suggest that the transcriptional program directed by *POU6f1* downstream of local CRH signaling in adult-born neurons influences circuit dynamics in response to activity-dependent peptide signaling in the adult brain.

Key words: adult-born neurons; CRH; development; neuropeptides; olfactory; synapse

Significance Statement

Elucidating mechanisms of plasticity in the adult brain is helpful for devising strategies to understand and treat neurodegeneration. Circuit plasticity in the adult mouse olfactory bulb is exemplified by both continued cell integration and synaptogenesis. We previously reported that these processes are influenced by local neuropeptide signaling in an activity-dependent manner. Here, we show that local corticotropin-releasing hormone (CRH) signaling induces dynamic gene expression changes in CRH receptor expressing adult-born neurons, including altered expression of the transcription factor *POU6f1*. We further show that *POU6f1* is necessary for proper dendrite specification and patterning, as well as synapse development and function in adult-born neurons. Together, these findings reveal a novel mechanism by which peptide signaling modulates adult brain circuit plasticity.

Introduction

The adult mammalian brain exhibits remarkable cellular and synaptic plasticity (Alvarez-Buylla and Temple, 1998; Ming and Song, 2005; Zhao et al., 2008). Although basic brain architecture is established at birth, sensory experience continually refines brain circuitry. In the adult rodent olfactory bulb (OB), this is accomplished in part by ongoing, activity-dependent integration of adult-born neurons (Corotto et al., 1994; Najbauer and Leon,

Received June 13, 2017; revised Dec. 11, 2017; accepted Dec. 21, 2017.

Author contributions: C.K.M., M.Y.K., I.H., and B.R.A. designed research; C.K.M., M.Y.K., I.H., A.E., Y.M., J.O.-G., D.C., B.P., and S.P. performed research; C.K.M., I.H., G.M., and B.R.A. contributed unpublished reagents/analytic tools; C.K.M., M.Y.K., Z.L., and B.R.A. analyzed data; C.K.M. and B.R.A. wrote the paper.

This work was supported by the McNair Medical Institute, the National Institute of Neurological Disorders and Stroke (NINDS)–National Institutes of Health (NIH; Grant 1F31NS092435–01A1 to C.K.M. and Grant R01NS078294 to B.R.A.), the Eunice Kennedy Shriver National Institute of Child Health and Human Development (NICHD)–NIH (Grant 5U54HD083092 to B.R.A.), the RNA *In Situ* Hybridization Core facility at BCM (with the expert assistance of

1995; Cummings et al., 1997; Fiske and Brunjes, 2001; Yamaguchi and Mori, 2005; Alonso et al., 2006; Mandairon et al., 2006), dynamic dendritogenesis (Saghatelyan et al., 2005; Yoshihara et al., 2012), new spine formation (Arenkiel et al., 2011), and sensory-dependent synaptic modulation (Gao and Strowbridge, 2009; Cauthron and Stripling, 2014). Therefore, the mouse OB represents a robust model system in which to investigate the mechanisms of neural circuit plasticity in adult brain tissue. Although it is well established that activity affects the integration and synaptogenesis of new neurons in the adult OB, the molecular signaling events that sculpt the bulb's circuitry in response to external stimuli are poorly understood.

We previously discovered that activity-dependent CRH signaling by local interneurons shapes continual refinement of adult OB circuitry. CRH-secreting interneurons reside within the external plexiform layer (EPL) of the bulb. These CRH interneurons are reciprocally connected to mitral cells (MCs) (Huang et al., 2013), which, together with tufted cells, comprise the principal excitatory cells of the OB. When excited by sensory input relayed via mitral/tufted (M/T) cells, EPL interneurons both provide inhibitory feedback onto MCs (Huang et al., 2013; Kato et al., 2013; Miyamichi et al., 2013) and locally secrete CRH (Huang et al., 2013; Garcia et al., 2014). Secreted CRH signals to CRHR1-expressing granule cells (GCs) (Garcia et al., 2014). Interestingly, much of the GC layer in adult OBs is populated by adult-born granule neurons, which migrate to the bulb from their birthplace in the subventricular zone (SVZ). As they undergo survival selection and integration, adult-born neurons upregulate expression of CRHR1. CRHR1 activation by locally secreted CRH drives expression of synaptic proteins in the bulb, promotes integration of adult-born neurons, and marks a developmental window in which sensory learning can broaden and reshape excitatory connections onto developing GCs (Quast et al., 2017). This suggests that signaling by neuropeptides such as CRH exert critical roles in adult brain plasticity. However, the transcriptional programs that govern the functional and morphological changes downstream of activity-dependent neuropeptide signaling remain unclear.

In the present study, we investigated gene expression changes downstream of CRHR1 activity in OB GCs. We found that CRHR1 activity modulated transcriptional cascades implicated in neuronal maturation and/or synaptic development. Of these, we found that CRH signaling dynamically regulates expression of the transcription factor POU Domain Class 6 Transcription Factor 1 (*POU6f1*). *POU6f1* is a member of the POU factor family of transcription factors (Andersen et al., 1993; Okamoto et al., 1993; Bulleit et al., 1994) that have been shown previously to regulate neural development (Latchman, 1999). Despite previous characterization of *POU6f1*, contributions to peptide signaling and how *POU6f1* influences ongoing circuit remodeling through adult neurogenesis remain unknown. Here, we generated two novel mouse models that harbor either an endogenous HA tag on *POU6f1*, or a conditional knock-out (cKO) allele of *POU6f1*, to investigate the expression patterns and functions of *POU6f1* in CRHR1$^+$ GCs of the OB. To examine the contributions of the *POU6f1* transcriptional program toward peptide-dependent circuit refinement, we implemented both loss- and gain-of-function approaches. Using electrophysiological recordings and cell-tracing analysis, we found that *POU6f1* modulates excitatory synaptic connections established onto CRHR1$^+$ neurons and influences dendritic branch patterning of CRHR1$^+$ neurons directly. Together, our studies reveal a novel pathway by which neuropeptide signaling activates transcriptional programs to govern cell and synaptic plasticity in the adult brain.

Materials and Methods

Experimental animals. Experimental animals were treated in compliance with the Department of Health and Human Services and Baylor College of Medicine (BCM) Institutional Animal Care and Use Committee guidelines. Mice were maintained on a 12 h light/dark cycle with access to rodent chow and water *ad libitum*. *CRHR1*$^{-/-}$ animals (Smith et al., 1998) were obtained from JAX (https://www.jax.org/strain/004454). The generation and transgene expression patterns of *CRHR1*-Cre (Garcia et al., 2014) and *CRHR1*-EGFP (Justice et al., 2008) mice were described previously. Generation of *POU6f1* cKO and *POU6f1*$^{HA/HA}$ mice are described below.

Generation of POU6f1$^{HA/HA}$ CRISPR knock-in mouse. A DNA template for *in vitro* transcription of a 20 nt single guide RNA (sgRNA) targeted to the C terminal end of *POU6f1* (5′- GAACGTCTTTCAGATCCCGT-3′) was produced by the BCM Mouse ES Cell Core via overlapping oligonucleotides and high-fidelity PCR (Bassett et al., 2013). *In vitro* transcription of the sgRNA was performed using the MEGA shortscript T7 kit (Thermo Fisher Scientific). The BCM Genetically Engineered Mouse Core microinjected Cas9 mRNA (100 ng/ml; Thermo Fisher Scientific), the sgRNA (20 ng/ml), and the single-stranded oligonucleotide donor DNA carrying the 3xHA peptide tag (5′-ACTGAAGAACA CCAGCAAGCTGAACGTCTTTCAGATCCCGtCTAGAGCGGCCGT TTACCCATACGATGTTCCTGACTATGCGGGCTATCCCTATGAC GTCCCGGACTATGCAGGATCCTATCCATATGACGTTCCAGAT TACGCTCCGGCCGCCCTCGAgTAGGGCTCAGTGTCAGCGTGT GCCGGCGCACTGTACTCTT-3′) with 40 bp arms of homology to the target genomic region (Integrated DNA Technologies; 100 ng/ml), in RNase-free 1× PBS into the cytoplasm of 200 pronuclear (0.5 d postcoitum, dpc) stage C57BL/6J embryos. Injected embryos were then implanted into pseudopregnant ICR females. Offspring were genotyped (n = 43) using the primer set: 5′-GCAGAACCTGATGGAGTTCG-3′ (F) and 5′-AAACCCCCTCCTTCCACAT-3′ (R). One homozygous founder female tested positive for the *POU6f1*^{HA} fusion-tagged allele and the *POU6f1*$^{HA/HA}$ homozygous genotype was verified by Sanger sequencing. The founder was bred with a wild-type C57BL/6 male mouse and progeny screened for transmission of *POU6f1*^{HA} at P14.

Generation of POU6f1 cKO mouse. To generate *POU6f1* knock-out mice, AB2.2 embryonic stem cells (ESCs) derived from the 129 SvEv strain (BCM Mouse ES Cell Core) were electroporated with a custom-designed linearized targeting vector harboring codirectional LoxP sites that flank exons 2–11 of *POU6f1*. DNA from electroporated ESC lines was digested with EcoNI and analyzed by Southern blot using a radiolabeled 3′ probe (flanking the arms of homology and external to the targeting vector) and by genomic PCR with the primer set: 5′-CATATATACCCGTCGCTTTGGTA-3′ (F) and 5′-AGTTTTTAAGGC-CCAGTCTCACT-3′ (R) to identify the 5′ end of the targeting vector. Three independently targeted cell lines were selected and microinjected into the C57BL/6 blastocysts to generate chimeric mice. Male chimeric mice were kept for breeding with female C57BL/6 mice to test germline transmission of the targeted *POU6f1* locus. Of the three lines of mice generated from these chimeras, two (from ESC clones 1F11 and 1G11)

Dr. Cecilia Ljungberg, and funding from NIH Grant 1S10 OD016167 and NICHD Grant 1U54 HD083092 to the Intellectual and Developmental Disabilities Research Center); and the National Cancer Institute–NIH (Grant CA125123 to the Dan L. Duncan Comprehensive Cancer Center). We thank Dr. Andrew Groves, Dr. Roy Sillitoe, and Kevin Ung for helpful discussion and critical input on this manuscript; the Baylor College of Medicine (BCM) Medical Scientist Training Program for training support; and the BCM Mouse ES Cell and Genetically Engineered Mouse Cores for assistance with CRISPR/Cas9 reagent production, mouse ES cell culture, and mouse production.

The authors declare no competing financial interests.

I. Herman's present address: Department of Pediatric Neurology at BCM, Texas Children's Hospital, Houston, TX 77030.

Y. Moayedi's present address: Department of Cellular Physiology and Cellular Biophysics, Columbia University, New York, NY10027.

Correspondence should be addressed to Dr. Benjamin R. Arenkiel, Dept. of Molecular and Human Genetics, Jan and Dan Duncan Neurological Research Institute, Baylor College of Medicine, Houston, TX 77030. E-mail: arenkiel@bcm.edu.

DOI:10.1523/JNEUROSCI.1641-17.2017

 0270-6474/18/381444-19$15.00/0

displayed stable germline transmission. Progeny generated from clone 1G11 were selected for breeding and experimentation. To verify Cre-recombined excision of exons 2–11, we PCR genotyped to detect the recombined band using the primer set: 5′-CATATATAC-CCGTCGCTTTGGTA-3′ (F) and 5′-ACAAAACTTCTCTCATC-CCAAGC-3′ (R).

Microarray experiments. For control and overactive CRH signaling groups: *CRHR1*-Cre mice were stereotaxically injected with either AAV-FLEX-EGFP or AAV-FLEX(CA)*CRHR1*::EGFP (both serotype 2/9), respectively. The FLEX configuration renders expression of the payload dependent upon Cre recombinase (Atasoy et al., 2008). pAAV-(CA)*CRHR1*::EGFP was described previously (Garcia et al., 2014). Briefly, it is a constitutively active variant of the *CRHR1* receptor (Nielsen et al., 2000) that encodes a moiety of the ligand fused to the active region of CRHR1. For the loss-of-CRH signaling group: *CRHR1*$^{-/-}$ animals were injected with AAV-FLEX-EGFP serotype 2/9. All animals ($n = 5$ per group) were adult males (6–8 weeks old) and were injected into the core OB with coordinates targeting the GC layer (GCL) (from bregma in mm: AP 3.92, ML 0.9, DV from surface of skull −2.88). Injection parameters were as follows: 20× 25 nl, 30 s apart, flow rate 23 nl/s. Animals were harvested 2 weeks after infection for RNA isolation. Whole OBs (~24 mg tissue per animal) were dissected and total RNA extracted using TRIzol reagent (Invitrogen) according to the manufacturer's protocol. RNA isolate was treated with DNase (Promega), followed by phenol–chloroform extraction. Purified RNA was quantified using a NanoDrop (NanoDrop Technologies).

Microarray hybridization and analysis. RNA samples were shipped to Miltenyi Biotec on dry ice for hybridization. RNA samples were quality-checked via the Agilent 2100 Bioanalyzer platform (Agilent Technologies). Then, 100 ng of each total RNA sample was used for the linear T7-based amplification step. RNA samples were amplified and Cy3-labeled using the Agilent Low Input Quick Amp Labeling Kit (Agilent Technologies) according to the manufacturer's protocol. Yields of cRNA and the dye-incorporation rate were measured with the ND-1000 Spectrophotometer (NanoDrop Technologies). Hybridization was performed according to the Agilent Technologies 60-mer oligo microarray processing protocol using the Agilent Gene Expression Hybridization Kit (Agilent Technologies). Fluorescence signals of the hybridized Agilent Technologies microarrays were detected using their microarray scanner system. Agilent Feature Extraction Software was used to read out and process the microarray image files. Statistical analyses were performed by Dr. Zhandong Liu (BCM and Texas Children's Neurological Research Institute). Expression fold changes between groups were considered significant at a false discovery rate of $q < 0.05$ when unpaired Student's t tests were corrected for multiple comparisons (Storey and Tibshirani, 2003). The datasets have been deposited in NCBI's Gene Expression Omnibus (Edgar et al., 2002) and are accessible through GEO Series accession number GSE98799 (https://www.ncbi.nlm.nih.gov/geo/query/acc.cgi?acc=GSE98799).

RNA in situ *hybridization (ISH)*. ISH was performed on 25 μm coronal OB sections from fresh-frozen adult *CRHR1*$^{+/+}$ or *CRHR1*$^{-/-}$ P90 male mouse brains. A digoxigenin-labeled mRNA antisense probe was designed against *POU6f1* using reverse-transcribed mouse cDNA as a template. The sequence for the custom-designed *POU6f1* probe was 5′-TCCTGTCTCNCCCCACCTCCCAAGCACTGGGTCTGCAGTCG CGTGCCACTGTGCCGCTGTGCCTGGCTCTTCTCCACTCCACAG CCTTACTGAGCTTGCTCTCTGGATGATGTTGACATCACGTGAT CTACCCTGAAGCAATGACTCTCAAACATGGACATGATGCAGA GACACCAGGGCTCAGCTTTCTCTCTCGTACCCTGTTCCCTTT CCTGGTCCTCTTGGGTCCTGCAGTACTGGTGTGGAGGGACCT CCTAGTAGCTCTGACAATGAGAGGAGGGCAGTTGTGTGCTG ATCACACACACACACACACACCACAAGTCTGTCAGGTATAAGG AGACAAGTAGGTTGCTTTCCTGATCCTGCCTCCCAAGAAAGAA TAATTCCCAGAGCGATTCTAGGTCATGTGATTATCATCCTGC TTCTGTGAGATGGAAGTCAGGAGGGGTCCTGTAAGAGAGCT TTCAGTAGGGATGCTTAGAGCCCTGAAGCTTATCAAGATGAT GCACCTGAGAAAACTATATGCAGATCTGCAGCTTTTCTTGCT CAAAGCCTGCACTCAGGAGGTACTACACAGTCAGCCATGCT GTGGTCAGCCATGCTGTGGTCAGCCATGCTGTGGACATGGG AGAGGATGCCATGCAGTCTATGCATGACAGGCGGGGATAAT CATGGCCCACTAAATTAAGCCGACCACTCGTTCTCACCC-3′. ISH was performed and tissue imaged by the RNA *In Situ* Hybridization Core at BCM using an automated robotic platform as described previously (Yaylaoglu et al., 2005). Slides were imaged and *post hoc* pseudocoloring for cellular *POU6f1* expression was performed using the Celldetekt protocol as described previously (Carson et al., 2005).

Luciferase reporter assay. The 686 bp *POU6f1* candidate promoter element was amplified from a template of purified mouse genomic DNA using a high-fidelity Taq (Roche 11732641001) and the primers 5′-gaaggtgggaaagcgagcta-3′ (F) and 5′-gcccgcagacaaagaagc-3′ (R) harboring KpnI and BamHI linkers, respectively. The amplicon was electrophoresed on a 1% agarose gel and purified using a kit (Qiagen 28704). The 66 bp element within the *POU6f1* candidate promoter containing the predicted CREB-binding site (5′-tgacgtcc-3′) was generated by annealing the forward oligo 5′-cacagctgctccggagaccctgagcctt agtgacgtccgagttccctctcctttacggcctagagg-3′ with the reverse oligo 5′-cctctaggccgtaaaggagagggaactcggacgtcactaaggctcagggtctccggagcagctgtg-3′, creating a double-stranded oligo, with 5′ KpnI and 3′ HindIII linkers. The 686 bp candidate promoter element and 66 bp CREB binding site-containing element were individually cloned into the pGL4.29-Luc2P reporter vector (Promega E8471) upstream of the firefly luciferase Luc2P gene. The promoter element vector and the CREB binding site-containing element vector were independently cotransfected with (CA)*CRHR1*, a constitutively active variant of *CRHR1* (Nielsen et al., 2000), or an empty vector control into Neuro2A cells (ATCC CCL-131) or MCF-7 cells (ATCC HTB-22, kindly gifted by Dr. Rachel Schiff). Cells were plated to subconfluence in a multiwell plate and transfected with Lipofectamine 2000 reagent (Thermo Fisher Scientific 11668027; for Neuro2A cells) or Lipofectamine LTX reagent (Thermo Fisher Scientific 15338100; for MCF-7 cells) according to manufacturer's protocol. The pRL-TK vector carrying a copy of the *Renilla* luciferase under control of the weakly expressed HSV thymidine kinase promoter (Promega E2241) was cotransfected in every well as a control for transfection efficiency. A vector containing Luc2P downstream of a promoter sequence that was ablated of all potential CREB binding sites served as the negative control. Forty-eight to 120 h after transfection, cell lysates were obtained. Activity of firefly luciferase (Fluc) and *Renilla* luciferase (Rluc) were measured for each lysate using a Dual Luciferase Reporter Assay kit (Promega E1910) to generate the single measurement for reporter activity in relative light units (RLUs) in a TD-20/20 luminometer. Comparisons were made by Student's t test or Kruskal–Wallis test as indicated. All experiments were performed in replicate with three to six wells per transfection condition.

Western blot analysis. Male *POU6f1*$^{HA/HA}$ mice were deeply anesthetized using isoflurane. Brain tissue was dissected and homogenized in ice-cold RIPA buffer with protease inhibitor (1:200; Roche 11873580001). Total protein from samples equalized by mass were separated on a 10% SDS-PAGE gel and transferred to a nitrocellulose membrane. The membrane was blocked in 1× TBS without Tween and with 5% nonfat dry milk for 1 h at room temperature, followed by overnight incubation with 1:1000 mouse anti-HA.11 (Covance MMS-101R-200) and 1:2500 rabbit anti-actin (Sigma-Aldrich A5060) in 0.1% TBST/5% milk. The next day, the membrane was washed with 0.1% TBST and incubated with 1:12500 goat anti-mouse (IRDye 800CW; Li-Cor 926-32210) and 1:12500 goat anti-rabbit secondary (IRDye 680RD, Li-Cor 926-68071) in 0.1% TBST/5% milk for 1 h at room temperature. The membrane was washed before visualization by near infrared imaging (Odyssey CLx; LiCor).

Immunohistochemistry. Animals were deeply anesthetized with isoflurane, followed by intracardial perfusion of ice-cold 1× PBS, pH 7.35, and 4% PFA/1× PBS. Brains were dissected and postfixed in 4% PFA for 2 h at room temperature before cryoprotection in 30% sucrose at 4°C for 2 d. Brains were then frozen in optimal cutting temperature compound (Thermo Fisher Scientific 4585) on dry ice and OBs coronally sectioned into 1× PBS at 25–30 μm using a cryostat (Leica CM1860). Free-floating OB sections were blocked in 0.3% Triton X-100/10% normal goat serum/1× PBS for 30 min at room temperature on a shaker and stained with rabbit anti-HA (1:250; Cell Signaling Technology C29F4), mouse anti-NeuN (1:500; Millipore MAB377), rabbit anti-GFAP (1:1000;

DAKO Z0334), rabbit anti-DCX (1:500; Cell Signaling Technology 4604), or rabbit anti-TBX21 (1:500; kindly gifted by Dr. Sachiko Mitsui, RIKEN Brain Science Institute) in the same blocking solution as above overnight at 4°C. The following day, sections were washed in 1× PBS twice for 15 min at room temperature on a shaker and then stained with (1:500) anti-rabbit Alexa Fluor-546 (Thermo Fisher Scientific) and (1:500) anti-mouse Alexa Fluor-633 (Thermo Fisher Scientific) in blocking solution for 1 h at room temperature on a shaker. Sections were again washed twice in 1× PBS and then mounted in Fluoromount-G (Southern Biotech) on glass slides for imaging on a Leica DM6000B microscope. For quantification of coexpression, serial epifluorescent images from 4 to 7 OB slices per mouse ($n = 3$ mice) were obtained and examined for coexpression of CRHR1-GFP, *POU6f1*::HA, or NeuN in the total GCL or the superficial GCL, as specified. For colocalization of CRHR-GFP with *POU6f1*::HA, CRHR-GFP cells were selected first in a single image visualized in the green fluorescence channel, followed by determination of expression of *POU6f1*::HA in a superimposed image visualized in the red fluorescence channel. For each analysis, 180–400 cells per animal were randomly selected and counted. Statistical comparison for coexpression of CRHR1 and *POU6f1*::HA in the total versus superficial GCL was made by Student's *t* test.

5-Ethynyl-2′-deoxyuridine (EdU) pulse labeling and POU6f1 coexpression or survival analysis. EdU injection was performed as described previously (Garcia et al., 2014). Briefly, adult male and female *POU6f1*$^{HA/HA}$ mice received four doses of EdU intraperitoneally (Invitrogen, 50 mg/kg) with each dose injected 2 h apart. Then, 8, 14, 21, 31, and 45 d postpulse (dpp), animals were killed and OBs sliced coronally at 30 μm for staining against EdU (Click-iT EdU Alexa Fluor 647 imaging; Thermo Fisher Scientific C10340) and *POU6f1*::HA (using the procedure described above). Analysis of adult-born neuron survival in the OBs of *CRHR1*-Cre; *POU6f1*$^{\Delta Exon2\text{-}11/\Delta Exon2\text{-}11}$ cKO animals was performed by pulse labeling adult-born neurons in > 4 wk old male and female mice, and sacrificing animals at 31–32 dpp for OB sectioning and staining against EdU. Comparisons for survival rates were made between cKO tissue to that obtained from *POU6f1*$^{floxed\ Exon2\text{-}11/floxed\ Exon2\text{-}11}$ littermates that did not inherit the *CRHR1*-Cre transgene.

Electrophysiology. For all groups, both male and female mice >4 wks of age were used. For the *POU6f1* loss-of-function group ($n = 12$): *CRHR1*-Cre; *POU6f1*$^{\Delta Exon2\text{-}11/\Delta Exon2\text{-}11}$ cKO mice were stereotaxically injected with AAV-FLEX-EGFP or AAV-FLEX-mRuby2 (both serotype DJ/8) to label CRHR1$^+$ cells lacking *POU6f1* for recording. For the control ($n = 7$ mice) and gain-of-function ($n = 8$ mice) groups: *CRHR1*-Cre mice were injected, respectively, with either AAV-FLEX-EGFP (or AAV-FLEX-mRuby2) or with AAV-FLEX-GFP::*POU6f1* (all serotype DJ/8). All mice were injected into the OB core to target the GCL (coordinates from bregma in mm: AP 3.7–3.92, ML 0.65–0.9, DV from pia −0.8–1.1). Injection parameters per OB were as follows: 10 × 69 nl, 10 s apart, flow rate at 69 nl/s. Animals were killed >14 d after infection and before animals reached 12 weeks of age.

Slice preparation and recordings. Animals were deeply anesthetized with isoflurane and perfused intracardially with ice-cold artificial CSF (ACSF) containing the following (in mM): 122 NaCl, 3 KCl, 1.2 NaH_2PO_4, 26 $NaHCO_3$, 20 glucose, 2 $CaCl_2$, and 1 $MgCl_2$ at 305–310 mOsm, pH 7.3. Brains were dissected, embedded in low-melting point agarose, sectioned to 300 μM on a microtome (VT1200; Leica) and placed in ice-cold oxygenated (5% CO_2, 95% O_2) dissection buffer containing the following (in mM): 87 NaCl, 2.5 KCl, 1.6 NaH_2PO_4, 25 $NaHCO_3$, 75 sucrose, 10 glucose, 1.3 ascorbic acid, 0.5 $CaCl_2$, and 7 $MgCl_2$. Sections were recovered (at least 30 min at 37°C) in oxygenated ACSF and then acclimated at room temperature for 10 min before recordings. After recovery, slices were placed in a recording chamber on a fixed stage of an upright microscope (SliceScope Pro 6000 platform; Scientifica) and perfused with oxygenated ACSF at room temperature. Labeled cells were identified by transmitted light (DIC) and fluorescent imaging with a CoolLED pE-100 470 nm (EGFP) or 565 nm (RFP) excitation light source, 49002- ET-EGFP (FITC/Cy2) or 41043-HcRed1 emission filters (Chroma Technology) and an optiMOS camera (QImaging) controlled by Micro-Manager version 1.4.22 software (University of California–San Francisco). Whole-cell voltage-clamp recordings were performed using a Multiclamp 700B amplifier (Axon CNS; Molecular Devices) at room temperature (25–27°C). Electrodes were prepared from borosilicate glass electrodes (outer diameter 1.5 mm) by a micropipette puller (Sutter Instruments), pulled to tip resistances between 4 and 7 MΩ, and filled with internal solution containing the following (in mM): 110 $CsMeSO_3$, 0.2 EGTA, 4 NaCl, 30 HEPES, 2 Mg-ATP, 0.3 Na-GTP, and 14 creatine phosphate, 300–310 mOsm, pH 7.3. Miniature excitatory postsynaptic events were recorded in oxygenated ASCF with the addition of 1 μM TTX and 20 μM gabazine. Neurons were held at −80 mV throughout the experiment. The recorded current was digitized at 20 kHz using a Digidata 1440A (Molecular Devices) and Clampex version 10.6.2.2 software (Molecular Devices) and stored on a PC hard disk. Offline analysis included filtering at 1 kHz and was performed using MiniAnalysis (Synaptosoft) and Clampfit version 10.0.0.3 software (Molecular Devices). Statistical comparisons were made by one-way ANOVA or Kruskal–Wallis test or by a two-sample Kolmogorov–Smirnov test, as indicated. *Post hoc* tests for ANOVA analysis included examinations for linear trends among the loss-of-function, control, and gain-of-function groups, Dunnett's multiple-comparisons test for ANOVA tests, and Dunn's multiple-comparisons test for Kruskal–Wallis tests. To test whether the proportion of total observed mEPSC decay time constants <2.5 ms or, separately, >4 ms changed for *POU6f1*-overexpressing neurons, we performed a χ^2 test (without Yates' correction) for deviations of these proportions from expected frequencies determined by recordings from control neurons.

Cell morphology analyses. Animal groups representing loss- and gain-of-function and control groups were established as above in electrophysiology experiments. Adult male and female mice ($n = 3$ per group) were injected using the same parameters as outlined above into the core of OBs with low-titer viruses to achieve single-cell labeling (for loss-of-function: AAV-FLEX-tdTomato, for gain-of-function: AAV-FLEX-GFP-2A-*POU6f1*, for control: AAV-FLEX-tdTomato). Animals were killed >14 d after infection.

Brain slice preparation and imaging. Animals were deeply anesthetized and killed using isofluorane, followed by intracardial perfusion of ice-cold 1× PBS, pH 7.35, and 4% PFA/1× PBS. Brains were dissected, postfixed in 4% PFA for 2 h at room temperature, and then transferred to ice-cold 1× PBS. OBs were mounted on a sectioning post in 2–3% low-melting point agarose and sectioned horizontally into 120–150 μm slices on a vibratome. If bulbs were injected with a GFP-containing virus, then the slices obtained were blocked with 0.3% Triton X-100/10% normal goat serum/1× PBS and then stained overnight at 4°C with rabbit anti-GFP (1:500; Synaptic Systems) and subsequently with (1:500) anti-rabbit Alexa Fluor-488 (Thermo Fisher Scientific). Images of labeled cells were obtained with a Leica TCS SPE confocal microscope with a 20× objective using a digital zoom of 1.25×. *Z*-stacks were collected at 1.01 μm intervals, covering the entire cell and all dendritic arbors, and images were rendered to Neurolucida 360 (MBF Bioscience) for tracing. Analysis was performed using Neurolucida Explorer (MBF Bioscience) by an experimenter blinded to genotype. Measurements for dendritic lengths, branch order, and branch number were compared by ordinary one-way ANOVA with *post hoc* tests for linear trend and Dunnett's multiple-comparisons test. Sholl analyses were compared using two-way ANOVA with *post hoc* Bonferroni's multiple-comparisons test.

Olfactory behavior. Adult male and female mice cKO (*CRHR1*-Cre; *POU6f1*$^{\Delta Exon2\text{-}11/\Delta Exon2\text{-}11}$) or control (*POU6f1*$^{floxed\ Exon2\text{-}11/floxed\ Exon2\text{-}11}$) were tested for Go/No-Go olfactory associative task learning ($n = 9$ control and $n = 12$ cKO mice) and short-term olfactory memory ($n = 8$ per group) deficits using described previously approaches (Garcia et al., 2014). Briefly, for Go/No-Go olfactory task learning, mice were water restricted 1 d before training. Mice were trained in an odorant delivery chamber equipped with infrared beam-break nose-poke ports (Med Associates). Using a stepwise paradigm to shape behavior, mice were trained to respond to the Go odor (hexanol) stimulus by seeking a water reward and to respond to the No-Go odor (butyric acid) stimulus by refraining from seeking the water reward. Rates of correct responses were tracked by blocks of 200 completed trials during the learning acquisition phase and performance between groups assessed by two-way ANOVA.

For short-term olfactory memory assays, animals were acclimated to a mock test chamber for 30 min before being individually placed inside the experimental odor chamber by an experimenter blinded to genotype. The chamber featured two odorant ports on opposite sides, each loaded with either a cotton tip applicator soaked in 100 μl of a test odorant diluted to 1% volume/volume in mineral oil or in 100 μl of pure mineral oil. The following odors comprised the odor test panel: iso-amyl acetate, carvone, eugenol, and anisole. At each port, IR beam break sensors detected and recorded the number and length of nose pokes to quantify olfactory investigation of novel odors or mineral oil. Each mouse was tested at time 0 (initial exposure to novel odor), 30, 60, 90, and 120 min for 10 min per trial. One odorant per day was tested for each mouse, with one time interval (30, 60, 90, or 120 min after initial presentation) observed, for a total of 4 odorants tested per mouse over the course of 4 d. Data were transmitted to an Arduino Uno board and a custom Arduino script was written to quantify the number of nose pokes per animal per port. Negative pressure was applied on both sides of the box to prevent passive diffusion of odors throughout the testing phase.

Experimental design and statistical analysis. All means are reported as means ± SE unless otherwise specified. Details including statistical analyses specific to each experiment are listed in appropriate subsections in Materials and Methods. A minimum number of animals to be used toward each experiment was determined by previous findings on the electrophysiological and morphological effects of altered CRH signaling on adult-born neurons in the OB (Garcia et al., 2014) and power analysis based on $\alpha = 0.05$ at 80% statistical power. Data were analyzed using Prism 6 (GraphPad Software) or Excel (Microsoft). For relevant datasets, before analysis, statistical outliers were identified by either Grubb's test for a single outlier (two tailed at $p < 0.05$) for $n < 25$ or Rosner's extreme studentized deviate test for multiple outliers (two tailed at $p < 0.05$) with a maximum number of outliers of 2 for $n \geq 25$ datasets, using internet-based software (http://contchart.com/outliers.aspx) and removed before comparisons. This procedure identified outliers each in the following datasets and groups for electrophysiology experiments: mEPSC frequency, control (×2) and overexpression (×2); mEPSC amplitude, cKO (×2); membrane resistance, cKO (×2), and control (×1). Removal of outliers did not change conclusions for mEPSC frequency or membrane resistance but did change the conclusion for mEPSC amplitudes (with two outliers in cKO group retained: Kruskal–Wallis test, $p = 0.1888$ vs with two outliers removed: one-way ANOVA, $p = 0.0481$). No outliers were detected for morphological datasets. Statistical comparisons between control and loss- or gain-of-function groups were made by ordinary one-way ANOVA or Kruskal–Wallis test as appropriate, followed by Dunnett's or Dunn's multiple-comparisons tests, respectively, as specified in the Results. For normally distributed electrophysiological and morphological data, we performed an additional *post hoc* test for linear trend among the groups for each dependent variable, when the groups were ordered by increasing levels of the independent variable (*POU6f1* expression in CRHR1$^+$ GCs): *CRHR1*-Cre;*POU6f1*$^{\Delta Exon2\text{-}11/\Delta Exon2\text{-}11}$; AAV-FLEX-GFP (cKO) representing low expression of *POU6f1*, *CRHR1*-Cre;AAV-FLEX-GFP (Control) representing endogenous expression of *POU6f1*, and *CRHR1*-Cre;AAV-FLEX-GFP::*POU6f1* (*POU6f1*) representing high expression of *POU6f1*.

Results

CRH signaling in the bulb is associated with gene expression changes

We showed previously that local CRH signaling functions as an activity-dependent cue for morphological and functional development of adult-born GCs in the OB (Garcia et al., 2014). As adult-born neurons mature into CRHR1-expressing GCs, olfactory learning influences their connectivity (Quast et al., 2017). Therefore, CRHR1 expression and synaptic input mark a developmental window for sensory-dependent refinement in the olfactory circuit. To determine how CRH signaling regulates the maturation of adult-born granule neurons mechanistically in the bulb, we queried the downstream transcriptional targets of altered levels of CRH signaling. Due to technical limitations of controlling expression of the small, secreted neuropeptide CRH, we established animal models of loss- and gain-of-function using genetically modified variants of the CRHR1 receptor (Fig. 1*A*, top).

We modeled loss of local CRH signaling by using a knock-out *CRHR1*$^{-/-}$ mouse line in which GCs of the OB lack functional *CRHR1* expression (Smith et al., 1998). To model endogenous or increased levels of CRH signaling, we used *CRHR1*-Cre transgenic animals (Garcia et al., 2014). *CRHR1*-Cre animals were stereotaxically injected with conditional adeno-associated viruses (FLEX) AAV (Atasoy et al., 2008) to target CRHR1$^+$ neurons selectively with either AAV-FLEX-EGFP (modeling endogenous levels of CRH signaling) or a FLEXed constitutively active (CA) version of *CRHR1* fused to EGFP [AAV-FLEX-(CA)*CRHR1*::EGFP; Nielsen et al., 2000; modeling overactive CRH signaling]. To control for the effects of viral infection on gene expression analysis, we also injected AAV-FLEX-EGFP into the bulbs of *CRHR1*$^{-/-}$ animals. All AAVs were injected into OBs using coordinates to target the GCL. Two weeks after injection, total bulb RNA was extracted from all 3 animal groups ($n = 5$ per group) and microarray hybridization was performed using Agilent Whole Mouse Genome Oligo Microarrays (8x60K, Design ID 028005).

To query the potential transcriptional targets of local CRH-dependent circuit refinement, we examined differential transcript expression in conditions of altered CRHR1 activity. Changes in transcript expression were considered significant when unpaired Student's *t* tests, corrected for multiple comparisons, had a false discovery rate (q) < 0.05 (Storey and Tibshirani, 2003). Of the transcripts for which expression patterns changed significantly in response to altered CRH signaling, we narrowed candidates for further study to those with reciprocal expression changes between loss- and gain-of-function animal models. This filter criterion focused our study on changes that were more likely to be in direct response to changes in CRH signaling and yielded a total of 57 genes with expression that changed dynamically and reciprocally when CRHR1 activity was altered. Interestingly, one of the most common cellular processes affected by reciprocally expressed transcripts was gene regulation (Fig. 1-1, available at https://doi.org/10.1523/JNEUROSCI.1641-17.2017.f1-1). This suggested that one major contribution of local CRH signaling in the bulb is to induce action of an array of gene regulators to direct adult-born neuron maturation and integration systematically.

Because we were interested in identifying the most upstream genetic changes related to CRH signaling in the bulb, we further focused our study toward genes implicated in direct transcriptional regulation. Of the transcription factors identified from our filter criteria, we observed the largest reciprocal expression changes for *POU6f1*. Relative to expression in *CRHR1*$^{-/-}$ bulbs, *POU6f1* expression was 5.28-fold higher in *CRHR1*-Cre;AAV-FLEX-EGFP control bulbs ($n = 5$ animals per group, q = 0.04) and 6.82-fold higher in (CA)*CRHR1* overactivation bulbs ($q = 0.0076$; Fig. 1*B*,*C*). This suggested that *POU6f1* transcription mirrors *CRHR1* expression and activity in the adult OB. *POU6f1* is a member of the POU factor family of transcription factors (Andersen et al., 1993; Okamoto et al., 1993), which regulate expression of developmental genes in the nervous system (Latchman, 1999). Expression of *POU6f1* is noted widely throughout the embryonic CNS (Cui and Bulleit, 1998) and adult CNS (Lein et al., 2007), yet its functions in both peptide signaling mediation and synaptic and circuit development in the adult brain have not been elucidated.

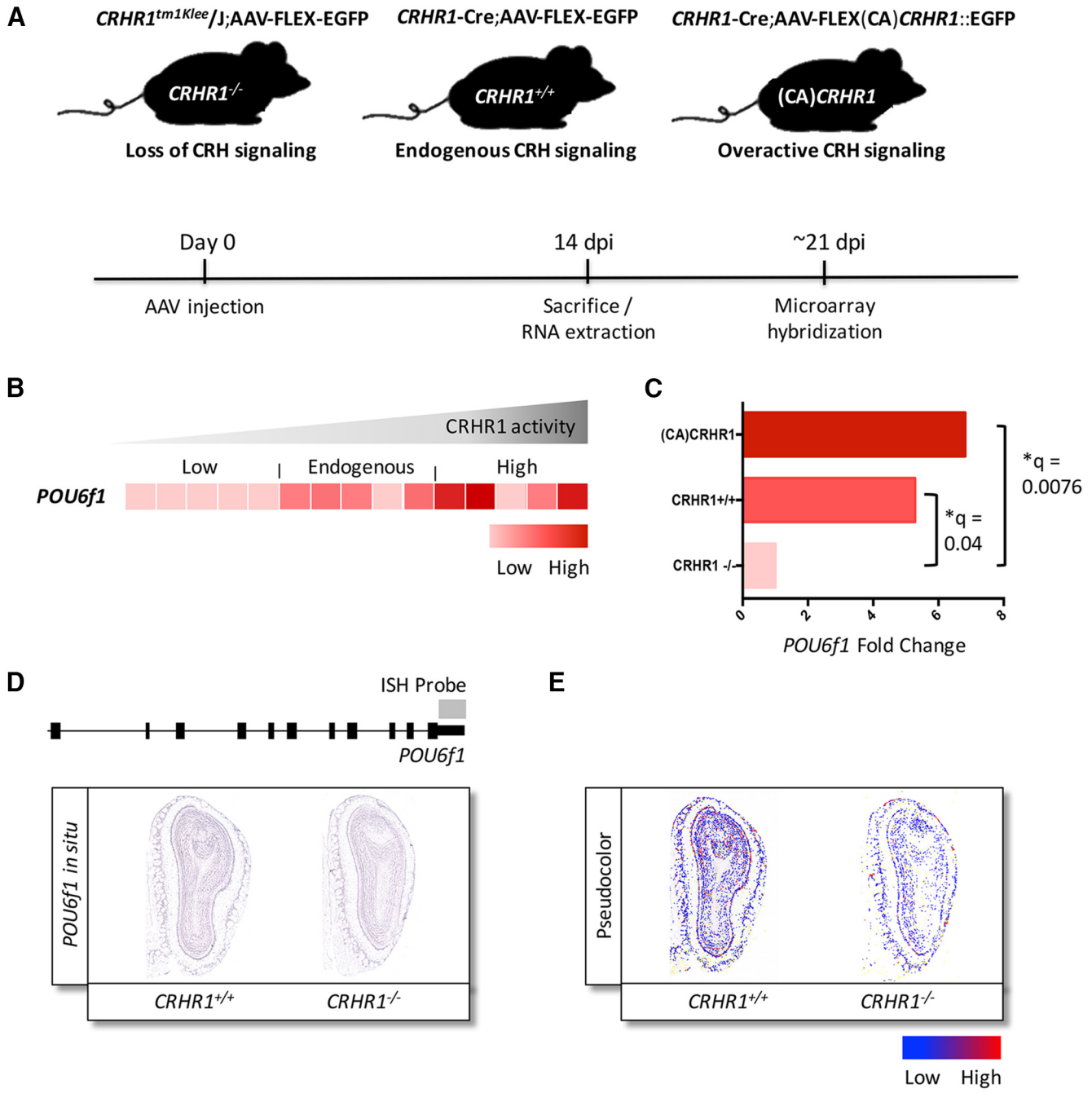

Figure 1. Local CRH signaling is associated with dynamic expression of the transcription factor *POU6f1*. ***A***, Top, Method of gene expression profiling. Three groups of animals were used to model changes in local CRH signaling in the bulb by viral and genetic manipulations: "loss of CRH signaling" group is represented by *CRHR1*$^{-/-}$ mice injected with AAV-FLEX-GFP; "endogenous CRH signaling" group is represented by *CRHR1*-Cre mice injected with AAV-FLEX-EGFP; and "overactive CRH signaling" group represented by *CRHR1*-Cre mice injected with AAV-FLEX-(CA)*CRHR1*::EGFP ($n = 5$ animals per group). Bottom, Experimental timeline. ***B***, Heatmap of microarray expression signals for *POU6f1* from bulbs with low, endogenous, or high levels of CRHR1 activity. Each colored box represents the normalized signal intensity obtained from an individual sample from each group (low = light pink, high = dark red; $n = 5$ animals per group). The full list of genes for which expression changed reciprocally in response to higher and lower levels of CRH signaling in the bulb and the cellular processes in which these genes are implicated are provided in Figure 1-1 (available at https://doi.org/10.1523/JNEUROSCI.1641-17.2017.f1-1). ***C***, Bar graph depicting estimated expression fold changes in *POU6f1* across experimental groups, assigning *CRHR1*$^{-/-}$ OBs as the reference sample (value of 1). A single value for expression fold change was derived across each group. Therefore, no variance or errors of estimation are shown. Relative to *POU6f1* expression in *CRHR1*$^{-/-}$ bulbs: bulbs with endogenous levels of CRHR1 activity expressed 5.28-fold higher levels of *POU6f1* ($q = 0.04$) and bulbs expressing (CA)*CRHR1* expressed 6.82-fold higher levels of *POU6f1* ($q = 0.0076$). Statistical comparisons were made by unpaired Student's *t* test corrected for multiple comparisons at a false discovery rate (q) (Storey and Tibshirani, 2003) as specified in the Materials and Methods. ***D***, Raw data from RNA *in situ* hybridization to detect *POU6f1* expression in coronal bulb sections from *CRHR1*$^{+/+}$ wild-type versus *CRHR1*$^{-/-}$ bulbs of adult male mice (P90). A custom probe was designed against the C terminal region of the gene and is represented as a gray bar above the exon-intron schematic of *POU6f1*. ***E***, Signal intensities from *in situ* hybridization in ***D*** were pseudocolored postprocessing to detect relative intensity of changes in *POU6f1* expression as specified in the Materials and Methods (lower levels of expression = blue, higher = red).

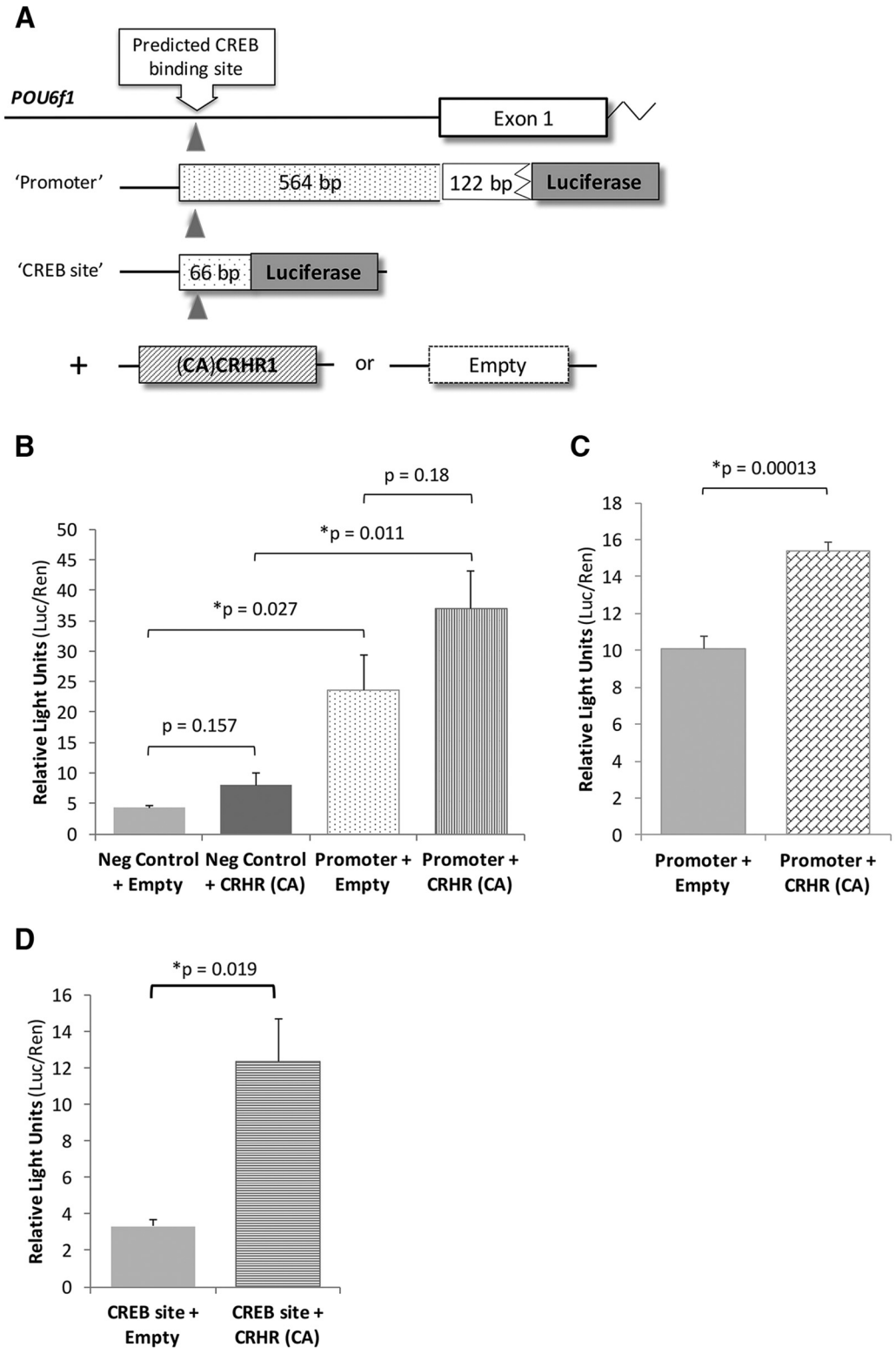

Figure 2. CRHR1 activity drives regulatory activation of *POU6f1*. ***A***, Luciferase reporter constructs used to test the interaction between CRHR1 activity and transcriptional activation of *POU6f1*. Two moieties, each containing the same predicted CREB-binding site, from the regulatory regions of *POU6f1* (gray triangle) were independently cloned upstream of the firefly luciferase reporter. The first reporter construct ("promoter," top) contained a 686 bp element (comprised of a 564 bp portion of the region immediately upstream of Exon 1 and a 122 bp segment of Exon 1) upstream of the luciferase reporter. The second construct ("CREB site," bottom) contained a 66 bp minimal sequence from the predicted *POU6f1* promoter that flanked the 8 bp predicted CREB-binding site. These vectors were independently transfected into cell lines with a plasmid that encoded either (CA)*CRHR1* [also *CRHR* (CA)] or an empty plasmid control. All wells additionally received a control pRL-TK vector carrying a copy of *Renilla* luciferase under control of the weakly expressed HSV thymidine kinase promoter as an internal control for transfection efficiency. ***B***, Luciferase reporter assay for "promoter" vector in Neuro2A cells. The negative control vector contained a minimal promoter element that was ablated of predicted CREB-binding sites upstream of the luciferase reporter. Negative control was cotransfected with either an empty plasmid or the plasmid encoding *CRHR* (CA; left two gray bars). Means for negative control + empty: 4.33 ± 0.33 RLUs versus negative control + *CRHR* (CA): 8 ± 2.08 RLUs, $p = 0.157$. Promoter vector was cotransfected with either an empty plasmid or the plasmid encoding *CRHR* (CA; right two patterned bars). Means for promoter + empty: 23.67 ± 5.67 RLUs versus promoter + *CRHR* (CA): 37 ± 6.11 RLUs, $p = 0.18$. Other comparisons [negative control + empty vs promoter + empty and (*Figure legend continues.*)

To verify the relationship of CRHR1 activity to *POU6f1* in the OB, we performed RNA *in situ* hybridization using a custom-designed probe against *POU6f1* in OB sections of $CRHR1^{+/+}$ or $CRHR1^{-/-}$ animals (Fig. 1*D*). In $CRHR1^{-/-}$ bulbs, lower *POU6f1* signal intensities, as determined by *post hoc* pseudocolor cell expression analysis (Fig. 1*E*), suggested that *POU6f1* expression declines in the absence of functional *CRHR1* expression. Therefore, we next sought to investigate whether CRHR1 activity promotes transcriptional activation of *POU6f1* directly.

CRH signaling promotes transcriptional activation of *POU6f1*

CRH-to-CRHR1 binding drives G_S-coupled signaling (Blank et al., 2003; Berger et al., 2006) and leads to cAMP-dependent gene transcription via phospho-activated cAMP-responsive element binding (CREB) protein (Giguère et al., 1982; Aguilera et al., 1983; Gonzalez and Montminy, 1989; Thiel and Cibelli, 1999) in the receptor-expressing cell. Interestingly, cAMP signaling has been shown to activate transcription of POU family factors related to *POU6f1* (Wang et al., 2009; Monuki et al., 1989) and the promoter region of *POU6f1* [Ensembl release 87] (Zerbino et al., 2015) harbors several potential CREB-binding sites, suggesting that *POU6f1* may be a direct target of cAMP signaling. The sequence 5′-TGACGTC*C*- 3′, located proximally upstream of the transcription start site of *POU6f1*, differs from the consensus CREB-binding site 5′-TGACGTC*A*-3′ (Montminy et al., 1986) by only the terminal base pair and thus functions as a potential CREB binding site.

To test whether CRHR1 activity regulates *POU6f1* transcription via a CREB-dependent mechanism, we cloned two separate vectors that contained elements from the regulatory region of *POU6f1* upstream of a luciferase enzyme. One vector comprised a 686 bp region at the 5′ end of the *POU6f1* gene, including the 564 bp immediately upstream of exon 1 and 122 bp of the 5′ segment of exon 1 (Fig. 2*A*, "promoter"). The second vector contained only the 66 bp region that immediately flanks the predicted CREB-binding site within the promoter region of *POU6f1* (Fig. 2*A*, "CREB site"). The "CREB site" reporter was comprised of the predicted CREB-binding site (8 bp) flanked by a total of 58 bp of genomic sequence unique to *POU6f1* (Kent, 2002). Both reporter vectors were independently cotransfected into Neuro2A or MCF-7 cells, each with either a construct encoding the constitutively active variant of *CRHR1* [(CA)*CRHR1*; Nielsen et al., 2000] or an empty control construct to test whether CRHR1-mediated cAMP signaling in cells altered activity of the regulatory components of *POU6f1*. To verify that observed changes in reporter activity in the presence of (CA)*CRHR1* were mediated via CREB binding, we also tested a negative control vector harboring the luciferase reporter downstream of a minimal promoter, in which all predicted CREB-binding sites had been mutated. Indeed, when this negative control vector was cotransfected with (CA)*CRHR1* into cells, no significant change in the level of reporter activity was observed relative to cotransfection of the negative control with an empty plasmid (unpaired Student's *t* test, $t_{(4)} = -1.74$, $p = 0.157$; Fig. 2*B*, left two solid gray bars). These data suggest that activity of *POU6f1*-regulatory elements induced by (CA)*CRHR1* was dependent on CREB binding.

Interestingly, transfection of the "promoter" vector into cells resulted in an increase in reporter activity versus the negative control vector (Fig. 2*B*; negative control + empty plasmid: 4.33 ± 0.33 relative light units or RLU versus promoter vector + empty plasmid: 23.67 ± 5.67 RLU, unpaired Student's *t* test, $t_{(4)} = -3.41$, $p = 0.027$, measurements on lysates obtained from 3 independent wells per transfection condition, means reported as means ± SE). This indicated that the *POU6f1* promoter showed basal activity in a neural cell line, consistent with the predicted role of *POU6f1* in developing brain cells (Bulleit et al., 1994). We further observed increased reporter activity when (CA)*CRHR1* was cotransfected with the "promoter" vector, but not with the negative control [Fig. 2*B*; negative control vector + (CA)*CRHR1*: 8 ± 2.08 RLU vs promoter vector + (CA)*CRHR1*: 37 ± 6.11 RLU, unpaired Student's *t* test, $t_{(4)} = -4.49$, $p = 0.011$], providing evidence of a synergistic interaction between CRHR1 activity and the *POU6f1* candidate promoter sequence in a neural cell line.

Unexpectedly, when the "promoter" vector was cotransfected with (CA)*CRHR1*, reporter activity was not significantly increased over basal activity of the "promoter" alone [Fig. 2*B*, right two bars; promoter vector + empty plasmid: 23.67 ± 5.67 RLUs vs promoter vector + (CA)*CRHR1*: 37 ± 6.11 RLU, unpaired Student's *t* test, $t_{(4)} = -1.6$, $p = 0.18$]. We reasoned that this resulted from either constitutively high basal promoter activity and/or the presence of other regulatory components within the promoter element that could mute the effect of (CA)*CRHR1*-associated activation.

To address whether reducing basal promoter activity in cells could clarify the relationship of (CA)*CRHR1* to activity of the candidate *POU6f1* promoter sequence, we identified the MCF-7 cell line (Soule et al., 1973), which has been reported to have low *POU6f1* expression as determined by RNA sequencing (Uhlén et al., 2015). MCF-7 cells were cotransfected with either the "promoter" vector plus (CA)*CRHR1* or empty vector control. Data from these experiments revealed a direct activation of the *POU6f1* promoter by constitutive CRHR1 activity in a cell line with low baseline *POU6f1* expression [Fig. 2*C*; promoter vector + empty plasmid: 10.1 ± 0.64 RLU versus promoter vector + (CA)*CRHR1*: 15.4 ± 0.45 RLU, Kruskal–Wallis test, $H(49) = 14.593$, $p = 0.00013$].

To address the possible presence of inhibitory components within the candidate *POU6f1* promoter that could lessen the effects of (CA)*CRHR1*, we cotransfected (CA)*CRHR1* or an empty vector control with the "CREB site" reporter vector (Fig. 2*A*) containing only 66 bp of the predicted *POU6f1* promoter (including the 8 bp CREB binding site) into the Neuro2A cell line. Because the "CREB site" reporter vector contained only a minimal segment of the predicted *POU6f1* promoter, we anticipated that when the "CREB site" vector was cotransfected with (CA)*CRHR1*, reporter activity would rise. Indeed, reporter activity increased significantly when the "CREB site" reporter plasmid was cotransfected with (CA)*CRHR1* [CREB site reporter vector + empty plasmid: 3.33 ± 0.33 RLU vs CREB site reporter vector cotransfected with (CA)*CRHR1*: 12.33 ± 2.33 RLU, unpaired Student's *t* test, $t_{(4)} = -3.82$, $p = 0.019$; Fig. 2*D*]. Together, these data suggest that activation of CRHR1 can initiate CREB-dependent transcriptional activation of *POU6f1* and that *POU6f1* is a *CRHR1*/cAMP-inducible transcription factor the expression

←

(*Figure legend continued.*) negative control + *CRHR*(CA) vs promoter + *CRHR*(CA)] are described in the Results. ***C***, Luciferase reporter assay for "promoter" vector in MCF-7 cells. Means for promoter + empty: 10.1 ± 0.64 RLUs versus promoter + (CA)*CRHR1*: 15.4 ± 0.45 RLUs, Kruskal–Wallis test, $p = 0.00013$. ***D***, Luciferase reporter assay for "CREB site" vector. Means for CREB site + empty: 3.33 ± 0.33 RLUs versus CREB site + *CRHR*(CA): 12.33 ± 2.33 RLUs, $p = 0.019$. Means are displayed as means ± SE. For all experiments, $n = 3$–6 independent wells per transfected construct pair. All comparisons were made by unpaired Student's *t* test unless otherwise specified.

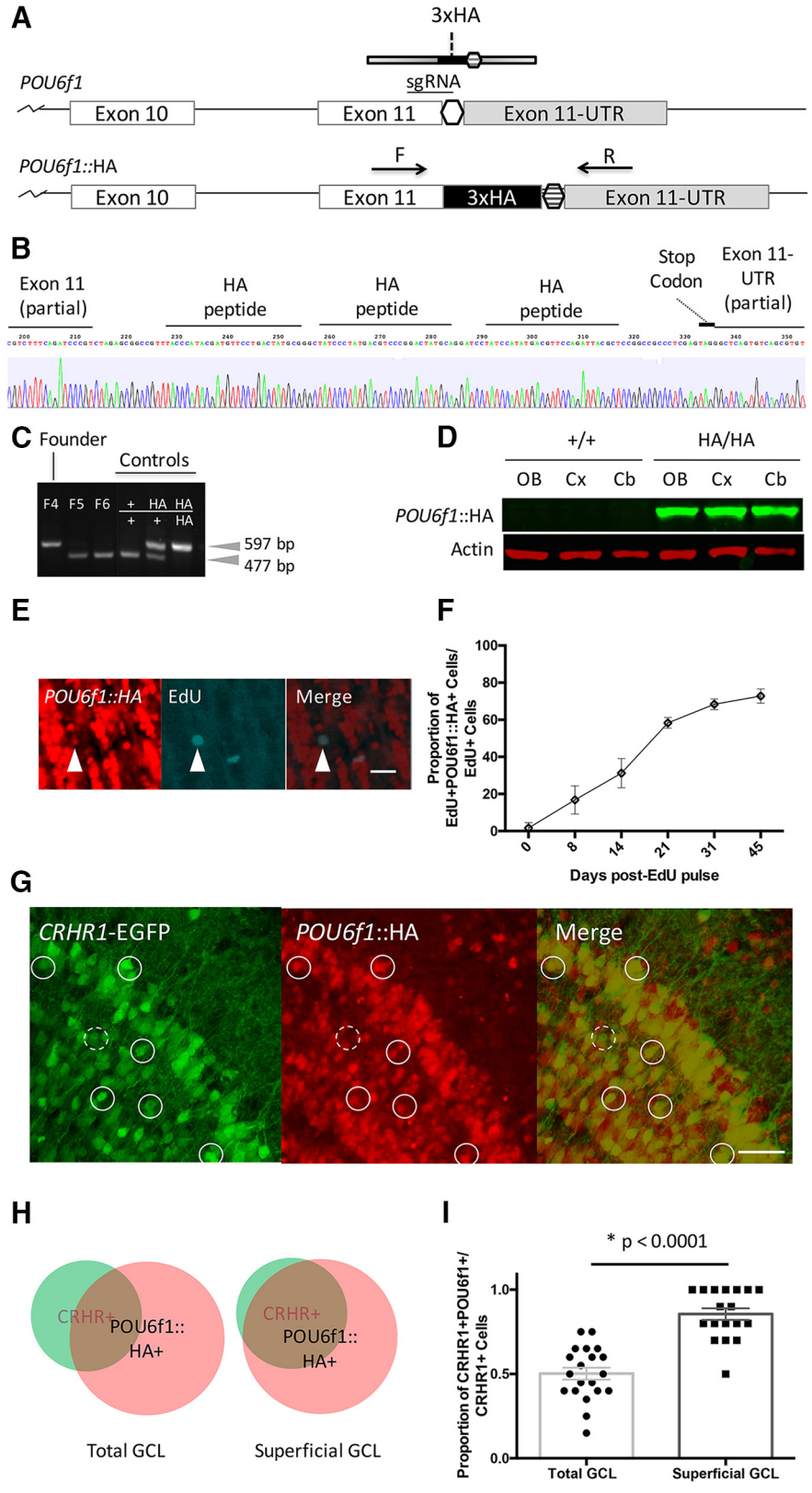

Figure 3. *POU6f1* is expressed by CRHR1 $^{+}$ GCs of the adult OB. ***A***, Approach to targeting *POU6f1* with an endogenously expressed 3xHA peptide tag by CRISPR knock-in. A 20 nt sgRNA was designed to target the C′ end of *POU6f1* upstream of the native stop codon (open hexagon). The homology-directed repair donor construct was a 200 nt single-stranded DNA oligomer that carried the sequence for the 3xHA peptide tag flanked by 40 bp arms of homology to *POU6f1*. Constructs were injected along with wild-type Cas9 mRNA into 200× 0.5 dpc mouse embryos before implantation into pseudopregnant female mice. Live-born pups were genotyped by PCR using primers (forward, F, and reverse, R) depicted as arrows (bottom), outside the arms of homology. UTR, Untranslated region. ***B***, Sanger sequencing and trace results from a purified PCR amplicon amplified using the primers depicted in ***A***. Results correspond to DNA from the *POU6f1* $^{HA/HA}$ founder animal ($n = 1$ of 43 live born pups) in ***C***. ***C***, Sample PCR genotyping results using primers specified in ***A*** from tail DNA obtained from live-born pups. One animal of 43 (2.3% of live-born pups) exhibited the predicted insertion of the 3xHA peptide tag and was used as the colony founder. The single 597 bp band for the founder animal indicates that both copies of the *POU6f1* gene were tagged in this animal (*POU6f1* $^{HA/HA}$). ***D***, Western blot demonstrating detection of the HA antigens fused to *POU6f1* in protein lysates taken from three brain regions of an adult *POU6f1* $^{HA/HA}$ animal (Cx, cortex, Cb, cerebellum; right three lanes, HA/HA), but not from lysates obtained from these regions in a *POU6f1* $^{+/+}$ littermate control (left three lanes, +/+). Actin was used as a loading control. ***E***, Representative images of EdU pulse-labled adult-born neurons costained for *POU6f1*::HA expression from *POU6f1* $^{HA/HA}$ OBs at the time points specified in ***F***. Scale bar, 25 μm. ***F***, Quantification of proportion of EdU-labeled adult-born neurons that express *POU6f1*::HA at specified time points in development (data points represent averages ± SEM, $n = 3$ animals per time point). ***G***, Representative image of the superficial GC layer of OB sections obtained from *CRHR1*-GFP; *POU6f1* $^{HA/HA}$ animals and stained for HA expression in colocalization analysis. Double-labeled cells (*CRHR1*-GFP $^{+}$ and *POU6f1*::HA $^{+}$) indicated with continuous line circles. Single-labeled cells (*CRHR1*-GFP $^{+}$ and *POU6f1*::HA $^{-}$) indicated with dotted line circles. Scale bar, 35 μm. ***H***, Diagram of coexpression of CRHR1 with *POU6f1*::HA in the total GCL versus superficial GCL of the adult OB. In the total GCL, 50.25 ± 7.4% of CRHR1 $^{+}$ GCs express *POU6f1*::HA and 22.75 ± 5.2% of *POU6f1*::HA $^{+}$ GCs express CRHR1. In the superficial GCL, 85.56 ± 7.3% of CRHR1 $^{+}$ GCs express *POU6f1*::HA and 66.67 ± 7.2% of *POU6f1*::HA $^{+}$ cells express CRHR1. ***I***, Quantification of proportion of coexpression of CRHR1 $^{+}$ and *POU6f1*::HA among CRHR1 $^{+}$ GCs selected from the total versus superficial GCL ($p < 0.0001$, unpaired Student's t test, $n = 3$ mice, 4–7 brain slices per mouse, $n = 180–400$ cells total counted). Means are ± SE.

of which in a developing neural cell can be mediated by external stimuli.

POU6f1 is expressed in CRHR1 $^{+}$ GCs *in vivo*

By microarray and *in situ* hybridization analyses (Fig. 1), we inferred a relationship between CRHR1 activity and *POU6f1* expression in the adult OB. Consistent with these data, *in vitro* luciferase reporter assays showed regulation of *POU6f1* expression by CRHR1 activation (Fig. 2). We next sought to reveal the relationship between *POU6f1* and CRHR1 expression in intact brain tissue. To avoid nonspecific labeling of POU6f1 from commercial antibodies (data not shown), we pursued a strategy of endogenously labeling *POU6f1* by epitope tagging. We used a CRISPR-based gene-targeting strategy (Cong et al., 2013) to generate a novel mouse line that harbors a multimeric hemagglutinin tag (3xHA) at the C-terminal end of *POU6f1*. For this, a 20 nt sgRNA and 200 nt single-stranded oligo donor template were

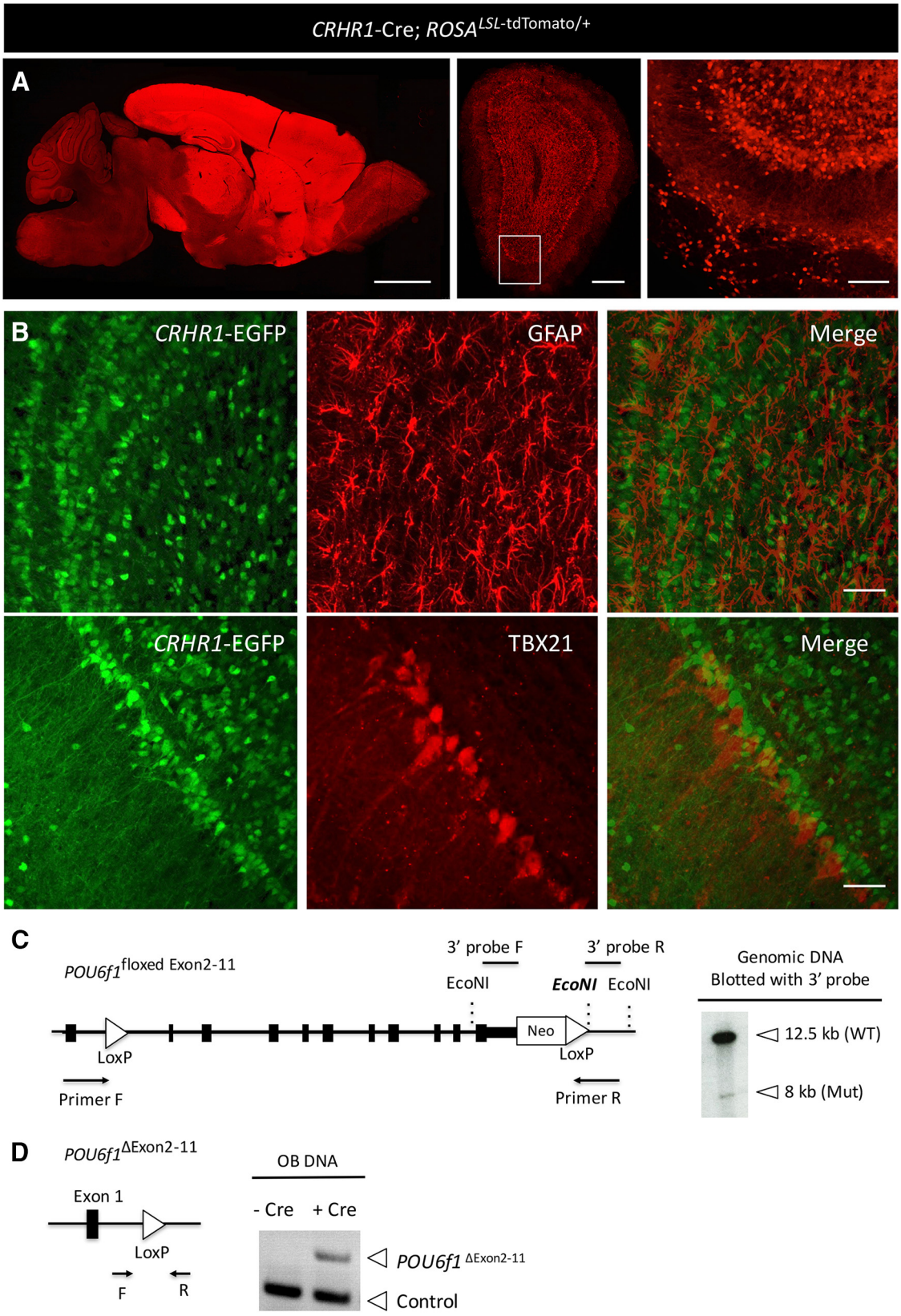

Figure 4. Generation of a *POU6f1* cKO transgenic animal line. ***A***, Micrograph of sagittal whole-brain (left) and coronal OB (middle, right) sections from an adult mouse expressing the *CRHR1*-Cre transgene and harboring one copy of the Cre-dependent conditional tdTomato reporter at the *ROSA* locus (*ROSA*$^{LSL\text{-}tdTomato/+}$). Scale bars, 1850 μM (left), 400 μM (middle), 75 μM (right). ***B***, Coexpression analysis of *CRHR1* and GFAP to mark glial cells (top) or *CRHR1* and TBX21 to mark projection neurons (bottom) in OBs of *CRHR1*-EGFP reporter mice (Justice et al., 2008). Scale bars, 50 μM. ***C***, Left, cKO-ready floxed *POU6f1* allele (*POU6f1*$^{floxed\ Exon2\text{-}11}$). Primers to generate the 3′ probe for Southern blotting to verify locus targeting are depicted as black lines above the schematic. The 3′ probe contained regions of the locus lying outside the arms of homology. The targeting vector introduced a novel 3′ EcoNI site (bold, italicized), which distinguishes the wild-type from the floxed *POU6f1* allele. Genotyping primers (depicted as arrows below the schematic) were designed upstream of the first LoxP site and downstream of the second LoxP site to verify Cre-mediated recombination. Right, Southern blot using probe against 3′ region of *POU6f1* hybridized to genomic DNA isolated from founder mouse and (*Figure legend continues.*)

designed to target endogenous *POU6f1* upstream of the native stop codon, creating a cut site for the insertion of the 3xHA sequence (Fig. 3*A*). Two hundred mouse embryos (0.5 dpc) were used for pronuclear injection of these components, along with wild-type Cas9 mRNA. Injected embryos were then implanted into pseudopregnant female mice. PCR-based genotyping and sequencing revealed that 1 of 43 (2.3%) live-born pups carried the correctly targeted, full sequence of 3xHA tagged *POU6f1* (Fig. 3*B*,*C*). This mouse was used as a founder to generate a colony of *POU6f1*$^{HA/HA}$ homozygote animals. Translation of the tagged-variant of *POU6f1* in the brains of *POU6f1*$^{HA/HA}$ animals was verified by Western blot, which detected the 3xHA peptide at the predicted molecular weight for 3xHA-tagged POU6f1 protein in the OB, cortex, and cerebellum of *POU6f1*$^{HA/HA}$ adult mouse brains (Fig. 3*D*).

To determine whether POU6f1 is expressed in CRHR1$^+$ GCs of the adult OB, we crossed the *POU6f1*$^{HA/HA}$ mouse line with a *CRHR1*-EGFP reporter mouse line (Justice et al., 2008) and stained OB sections obtained from *CRHR1*-EGFP; *POU6f1*$^{HA/HA}$ mice for HA antigen. Colocalization analysis of CRHR1$^+$ cells selected randomly from the total GCL showed that 50.25 ± 7.4% of CRHR1$^+$ cells are *POU6f1*::HA$^+$ ($n = 3$ mice, 4–7 brain slices per mouse, $n = 400$ cells total counted, means reported as ± 95% confidence interval), suggesting that CRHR1 activation *in vivo* may drive expression of *POU6f1* in only a subset of CRHR1-expressing GCs.

POU6f1 has been hypothesized to be involved in maturation of developing neurons in culture (Bulleit et al., 1994). Therefore, we reasoned that CRHR1$^+$POU6f1::HA$^+$ cells may represent olfactory GCs in later stages of development than CRHR1$^+$ POU6f1::HA$^-$ cells. To determine whether expression of POU6f1 is associated with a specific developmental stage, we costained GCs for *POU6f1*::HA and NeuN, a marker for mature neurons (Mullen et al., 1992). We found that 96.25 ± 3.4% of *POU6f1*::HA$^+$ cells are NeuN$^+$ and 94.38 ± 3.6% of NeuN$^+$ cells are *POU6f1*::HA$^+$, suggesting that POU6f1 is correlated with maturity in neurons. Further, to examine how *POU6f1*::HA expression changed through development of adult-born neurons, we pulse-labeled adult-born neurons with the thymidine analog EdU and costained for EdU and *POU6f1*::HA from birth through integration (Fig. 3*E*,*F*). The proportion of EdU-labeled adult-born neurons that expressed *POU6f1*::HA was very low on the day of pulsing (1.67 ± 1.67% at 0 dpp) and increased progressively over time (16.79 ± 4.39% at 8 dpp, 31.19 ± 4.52% at 14 dpp, 58.33 ± 1.67% at 21 dpp, 68.33 ± 1.67% at 31 dpp, and 72.81 ± 2.19% at 45 dpp). This steady increase in *POU6f1*::HA expression by adult-born GCs over time as GCs migrate functionally mature inside the bulb supported the notion that *POU6f1*::HA expression is correlated with neuronal maturity.

Interestingly, the localization patterns of CRHR1$^+$POU6f1::HA$^+$ versus CRHR1$^+$POU6f1::HA$^-$ GCs within the GCL suggested that *POU6f1* may alter other aspects of neuronal fate and/or maturation in CRHR1-expressing neurons. We observed that the majority of double-labeled GCs localized to the superficial regions of the GCL (Fig. 3*G*). Others have shown that the superficial GCL is enriched for long-surviving (Lemasson et al., 2005; Imayoshi et al., 2008) granule neurons with abundant synaptic connections (Orona et al., 1983, 1984). Superficial GCs also display distinct electrophysiological profiles relative to GCs deeper within the core of the bulb (Carleton et al., 2003). We therefore reasoned that CRHR1$^+$POU6f1::HA$^+$ cells may be earmarked for a functional fate distinct from that of CRHR1$^+$POU6f1::HA$^-$ cells. In consideration of this, we investigated whether POU6f1::HA expression in CRHR1$^+$ neurons was increased in the superficial GCL relative to CRHR1$^+$ neurons selected at random (from the "total" GCL). Whereas approximately half of randomly selected CRHR1$^+$ cells in the total GCL coexpressed *POU6f1*::HA, that ratio increased significantly in the superficial GCL, where abundant synapses are found (50.25 ± 7.4% colocalization in the total GCL vs 85.56 ± 7.3% in the superficial GCL, Fig. 3*H*, right, *I*; unpaired Student's *t* test, $t_{(36)} = 7.106$, $p < 0.0001$, $n = 3$ mice, 5–7 brain slices per mouse, $n = 180$ cells total counted). Enrichment of CRHR1$^+$*POU6f1*::HA$^+$ colabeling in synapse-rich regions of the GCL supported the possibility that CRHR1$^+$POU6f1::HA$^+$ cells may be functionally distinct from those that express CRHR1 alone. We note that the above results do not distinguish whether *POU6f1* could broadly promote neuronal maturation or specifically promote of a specific functional fate in CRHR1$^+$ GCs. In either of these cases, however, we predicted that *POU6f1* expression would affect the synaptic connectivity of adult-born CRHR1$^+$ GCs.

POU6f1 influences synaptic formation and connectivity in CRHR1$^+$ neurons

Having established that CRHR1$^+$*POU6f1*::HA$^+$ neurons selectively populate OB regions enriched for the formation (Orona et al., 1983, 1984) and long-term maintenance of synapses (Lemasson et al., 2005; Imayoshi et al., 2008), we next sought to determine the effects of altered *POU6f1* expression on synaptic connectivity. For this, we generated models of both loss- and gain-of-*POU6f1*-function, again using *CRHR1*-Cre transgenic mice (Garcia et al., 2014) to target CRHR1$^+$ neurons for *POU6f1* knock-out or overexpression, respectively. Target cells in the bulb were verified independently by crossing *CRHR1*-Cre mice to a *ROSA*$^{LSL\text{-}tdTomato}$ reporter line, which revealed the vast majority of fluorescent reporter expression in the bulb to be within GCs (Fig. 4*A*, right). Scattered periglomerular cells were also labeled, consistent with the small population of adult-born neurons that adopts this cell fate in the OB (Luskin, 1993; Ming and Song, 2005). To determine further the specificity of *CRHR1* expression by GCs, we examined coexpression of *CRHR1* and GFAP, a marker of glial cells (Fig. 4*B*, top), or TBX21, a marker of M/T cells (Fig. 4*B*, bottom), in OB sections prepared from *CRHR1*-EGFP reporter mice (Justice et al., 2008). These data affirmed that the primary cell population targeted by our manipulations in *CRHR1*-Cre mice was granule neurons of the OB.

For loss-of-function studies, we crossed *CRHR1*-Cre transgenic mice to a novel *POU6f1* cKO-ready (*POU6f1*$^{floxed\ Exon2\text{-}11}$) mouse line (Fig. 4*C*) to generate *CRHR1*-Cre; *POU6f1*$^{\Delta Exon2\text{-}11/\Delta Exon2\text{-}11}$ cKO animals. cKO mice harbored a recombined floxed *POU6f1* allele excised of exons 2–11, including the DNA-binding domain (Wey et al., 1994), in CRHR1$^+$ cells (Fig. 4*D*).

For gain-of-function studies, *CRHR1*-Cre animal OBs were stereotaxically injected with AAV carrying a Cre-dependent copy of *POU6f1* cDNA fused to a GFP marker (AAV-FLEX-GFP::*POU6f1*) or GFP alone (AAV-FLEX-GFP) as a control (Fig. 5*A*). CRHR1 expression in adult-born GCs is detected at approximately day 14 after birth in the SVZ (Garcia et al., 2014), which

←

(*Figure legend continued.*) digested with EcoNI. ***D***, Left, Predicted Cre-recombined allele (*POU6f1*$^{\Delta Exon2\text{-}11}$). Right, Genotyping primers shown in ***C*** were used to detect the recombined allele of *POU6f1* in the presence of Cre recombinase (left lane, OB DNA from a *CRHR1*$^{+/+}$;*POU6f1*$^{floxed\ Exons\ 2\text{–}11}$ mouse vs right lane, OB DNA from a *CRHR1*-Cre$^{Tg/+}$; *POU6f1*$^{\Delta Exon2\text{-}11/\Delta Exon2\text{-}11}$ littermate).

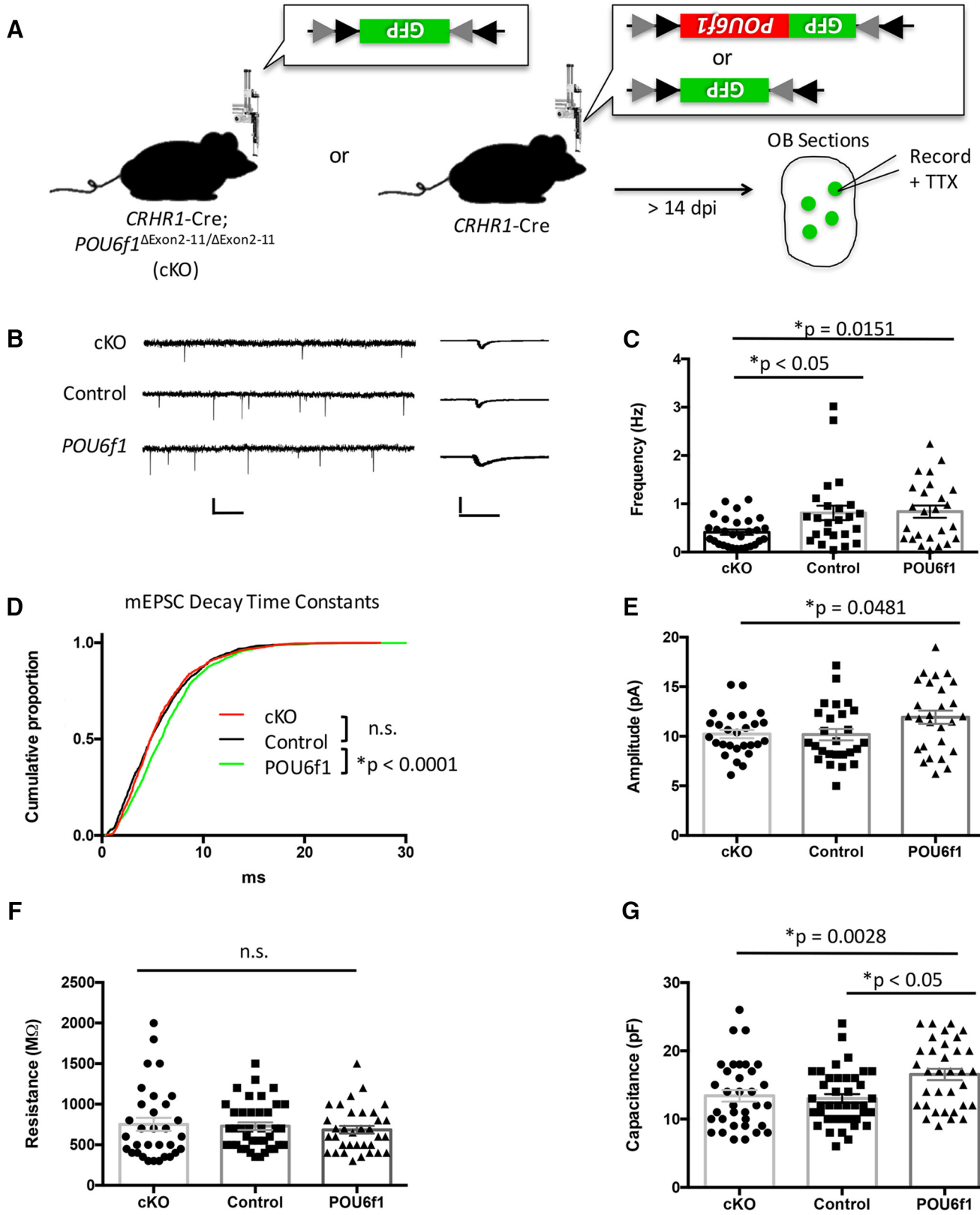

Figure 5. *POU6f1* influences functional maturation of CRHR1$^+$ neurons. ***A***, Generation of *POU6f1* loss-of-function (cKO), control (*CRHR1*-Cre;AAV-FLEX-GFP), and gain-of-function (*CRHR1*-Cre; AAV-FLEX-GFP::*POU6f1*) groups for analysis of the effects of *POU6f1* on miniature EPSCs (mEPSCs) onto CRHR1$^+$ neurons. All mice were injected with a Cre-dependent vector to ensure recording from labeled neurons of the same molecular subtype (CRHR1$^+$) across groups. Recordings were performed in the presence of 1 μM TTX to eliminate action potential-driven circuit activity. ***B***, Representative traces from GCs of each experimental group (left). Scale bars, 10pA, 1 s. Averaged traces from GCs from each experimental group (right). Scale bars, 20pA, 18ms. ***C***, Comparisons of mEPSC frequency. cKO mean: 0.41 $\pm$ 0.055 Hz, control mean: 0.811 $\pm$ 0.15 Hz, *POU6f1* overexpression mean: 0.838 $\pm$ 0.13 Hz ($p = 0.0151$, Kruskal–Wallis test, *post hoc* Dunn's multiple-comparisons test: $p < 0.05$ for the difference between cKO and control groups. cKO: $n = 12$ animals, $n = 29$ cells, control: $n = 7$ animals, $n = 24$ cells, *POU6f1* overexpression: $n = 8$ animals, $n = 25$ cells). Outliers were identified and removed from the control and overexpression groups, but doing so did not change the results of analysis (see Materials and (*Figure legend continues.*)

coincides with activity-dependent selection (Yamaguchi and Mori, 2005; Mouret et al., 2008; Kelsch et al., 2009). Therefore, our manipulations specified either cell-type-specific cKO or overexpression of *POU6f1* at this period in development for adult-born neurons.

To determine whether and how *POU6f1* expression altered synaptic inputs onto CRHR1$^+$ neurons, we performed whole-cell voltage-clamp recordings from labeled CRHR1$^+$ GCs in the presence of the sodium channel blocker tetrodotoxin (TTX). TTX blocks action potential-driven circuit activity, so its application isolates small subthreshold currents that are transmitted via synaptic inputs onto patched cells. We analyzed the frequency and amplitudes of currents recorded in TTX from patched CRHR1$^+$ cells to reveal quantal features of their synaptic contacts. Because a major contribution of GCs to odor processing is to shape bulb output via reciprocal, dendrodendritic connections with excitatory M/T cells (Jahr and Nicoll, 1980; Isaacson and Strowbridge, 1998), we focused on how altered *POU6f1* expression within GCs influenced excitatory currents back onto GCs. mEPSC recordings were performed from CRHR1$^+$ GCs labeled with a Cre-dependent vector, AAV-FLEX-GFP for cKO and control animals, AAV-FLEX-GFP::*POU6f1* for gain-of-function animals, to restrict our cross-group comparisons to granule neurons of a specific (CRHR1$^+$) subpopulation in the OB.

With altered *POU6f1* expression in CRHR1$^+$ neurons, we detected a significant change in the mEPSC frequency among loss-of-function, control, and gain-of-function groups (Kruskal–Wallis test, $H_{(2)} = 8.382$, $p = 0.0151$). Neurons that lacked *POU6f1* showed a decreased frequency of mESPCs (0.41 ± 0.055 Hz) compared with controls (0.811 ± 0.15 Hz; Fig. 5*B*,*C*; $p < 0.05$, Dunn's multiple-comparisons posttest, cKO group: $n = 12$ animals, $n = 29$ cells, control: $n = 7$ animals, $n = 24$ cells, means reported as means ± SE), suggesting that *POU6f1* expression is required for CRHR1$^+$ neurons to establish the normal repertoire of excitatory connections. Although the frequency of mEPSCs was higher for *POU6f1*-overexpressing neurons (0.838 ± 0.13 Hz for *POU6f1*-overexpressing cells vs 0.811 ± 0.18 Hz for controls), this difference did not reach significance ($p > 0.05$, Dunn's multiple-comparisons posttest, *POU6f1* overexpression group: $n = 8$ animals, $n = 25$ cells).

We next investigated whether *POU6f1* influences other properties of excitatory synapses that are made onto GCs. GCs receive excitatory input from M/T cells via dendrodendritic connections in the EPL and via axodendritic connections from M/T cell collaterals in the GCL (Shepherd et al., 2004). The disparate distances of these synapses from GC somas influence recorded electrophysiological properties, including excitatory current decay time constants (τ_{decay}; Schoppa, 2006). Dendrodendritic M/T cell synapses onto GCs exhibit currents with longer τ_{decay} values relative to more proximal axodendritic M/T cell synapses. Therefore we reasoned that significant changes in τ_{decay} distributions for mEPSCs recorded from *POU6f1*-overexpressing GCs could suggest a difference in the type of M/T connections established onto these cells. Because the majority of GCs display a mix of excitatory inputs (Schoppa, 2006), we examined the distributions of τ_{decay} from randomly sampled populations of mEPSC events across experimental groups.

Analysis showed a right shift in the distribution of τ_{decay} values for mEPSCs recorded from *POU6f1*-overexpressing neurons versus controls (Fig. 5*D*; two-sample Kolmogorov–Smirnov test, $p < 0.0001$, control group: $n = 7$ animals, $n = 26$ cells, 50 events per cell, *POU6f1* overexpression group: $n = 8$ animals, $n = 27$ cells, ~50 events per cell). Therefore, more mEPSCs onto *POU6f1*-overexpressing CRHR1$^+$ GCs displayed larger τ_{decay} values versus mEPSCs onto control CRHR1$^+$ GCs. No significant change in the distribution of τ_{decay} values was found between cKO and control mEPSCs (two-sample Kolmogorov–Smirnov test, $p = 0.1542$, control: $n = 7$ animals, $n = 26$ cells, 50 events per cell, cKO: $n = 12$ animals, $n = 27$ cells, ~50 events per cell). This suggested that *POU6f1*-overexpressing CRHR1$^+$ GCs gain excitatory input from synapses with decay kinetics similar to those of dendrodendritic M/T cell synapses (and/or those further away from the soma). Together with the above findings, these data suggest the possibility that, although loss of *POU6f1* may indiscriminately reduce the quantal content of excitatory connections onto developing GCs, increased *POU6f1* levels may enhance the quantal content of particular types of excitatory connections. However, this idea would require further experimentation and analysis to substantiate.

In our experiments, levels of *POU6f1* expression in CRHR1$^+$ cells also linearly affected the amplitudes of mEPSCs across cKO (10.23 ± 0.42 pA), control (10.17 ± 0.57 pA), and *POU6f1*-overexpressing (11.93 ± 0.67 pA) neurons (Fig. 5*E*; one-way ANOVA, $F_{(2,77)} = 3.156$, $p = 0.0481$, animals per group as above, cKO: $n = 27$ cells, control: $n = 26$ cells, *POU6f1* overexpression: 27 cells; posttest for linear trend, $R^2 = 0.05532$, $p = 0.035$). Although differences between the groups did not reach statistical significance in pairwise comparisons against controls ($p > 0.05$, Dunnett's multiple-comparisons test for both cKO vs control and *POU6f1*-overexpression vs control), the observed subtle but linear increase in mEPSC amplitudes in response to increasing levels of *POU6f1* could reflect a modest role for *POU6f1* in influencing the quantal size of excitatory synapses onto CRHR1$^+$ neurons. The above results suggest that *POU6f1* could influence multiple properties of excitatory inputs onto CRHR1$^+$ GCs.

We next sought to determine whether *POU6f1* influenced passive membrane properties of CRHR1$^+$ GCs. No differences were observed in membrane resistance among groups (Fig. 5*F*; cKO mean: 751.6 ± 79.9 MΩ, control mean: 729.5 ± 46.6 MΩ, *POU6f1*-overexpression mean: 685.3 ± 47.5 MΩ; Kruskal–Wallis test, $H_{(2)} = 0.636$, $p = 0.7256$, cKO: $n = 12$ animals, $n = 32$ cells, control: $n = 7$ animals, $n = 39$ cells, *POU6f1*-overexpression: $n = 8$ animals, $n = 34$ cells). Similarly, no difference in

←

(*Figure legend continued.*) Methods). ***D***, Cumulative mEPSC decay time constants. ($p < 0.0001$, two-sample Kolmogorov–Smirnov, or KS, test for the difference between distributions of the control versus *POU6f1* overexpression groups; for the difference between cKO and control groups, $p = 0.1542$ by two sample KS test; control: $n = 7$ animals, $n = 26$ cells, ~50 events per cell, *POU6f1* overexpression: $n = 8$ animals, $n = 27$ cells, ~50 events per cell). ***E***, Comparisons of mEPSC amplitudes. cKO mean: 10.23 ± 0.42 pA, control mean: 10.17 ± 0.57 pA, *POU6f1* overexpression mean: 11.93 ± 0.67 pA. ($F_{(2,77)} = 3.156$, $p = 0.0481$, ordinary one-way ANOVA. Dunnett's *post hoc* multiple-comparisons test did not reveal significant pairwise differences between groups; *post hoc* linear trend $R^2 = 0.05532$, $p = 0.035$. cKO: $n = 12$ animals, $n = 27$ cells, control: $n = 7$ animals, $n = 26$ cells, *POU6f1* overexpression: $n = 8$ animals, $n = 27$ cells.) Outliers were identified and removed from the cKO group before comparisons (see Materials and Methods). ***F***, Quantifications of membrane resistance. cKO mean: 751.6 ± 79.9 MΩ, control mean: 729.5 ± 46.6 MΩ, *POU6f1* overexpression mean: 685.3 ± 47.5 MΩ ($p = 0.7256$, Kruskal–Wallis test, cKO: $n = 12$ animals, $n = 32$ cells, control: $n = 7$ animals, $n = 39$ cells, *POU6f1* overexpression: $n = 8$ animals, $n = 34$ cells.) Outliers were identified and removed from the cKO and control groups but doing so did not change the results of analysis (see Materials and Methods). ***G***, Comparisons of membrane capacitance. cKO mean: 13.41 ± 0.85 pF, control mean: 13.03 ± 0.63 pF, *POU6f1* overexpression mean: 16.53 ± 0.83 pF. $F_{(2,105)} = 6.236$, $p = 0.0028$, ordinary one-way ANOVA; $p < 0.05$ for the difference between control and *POU6f1* overexpression groups by *post hoc* Dunnett's multiple-comparisons test. *Post hoc* linear trend $R^2 = 0.06733$, $p = 0.0059$.) Means displayed as mean ± SE.

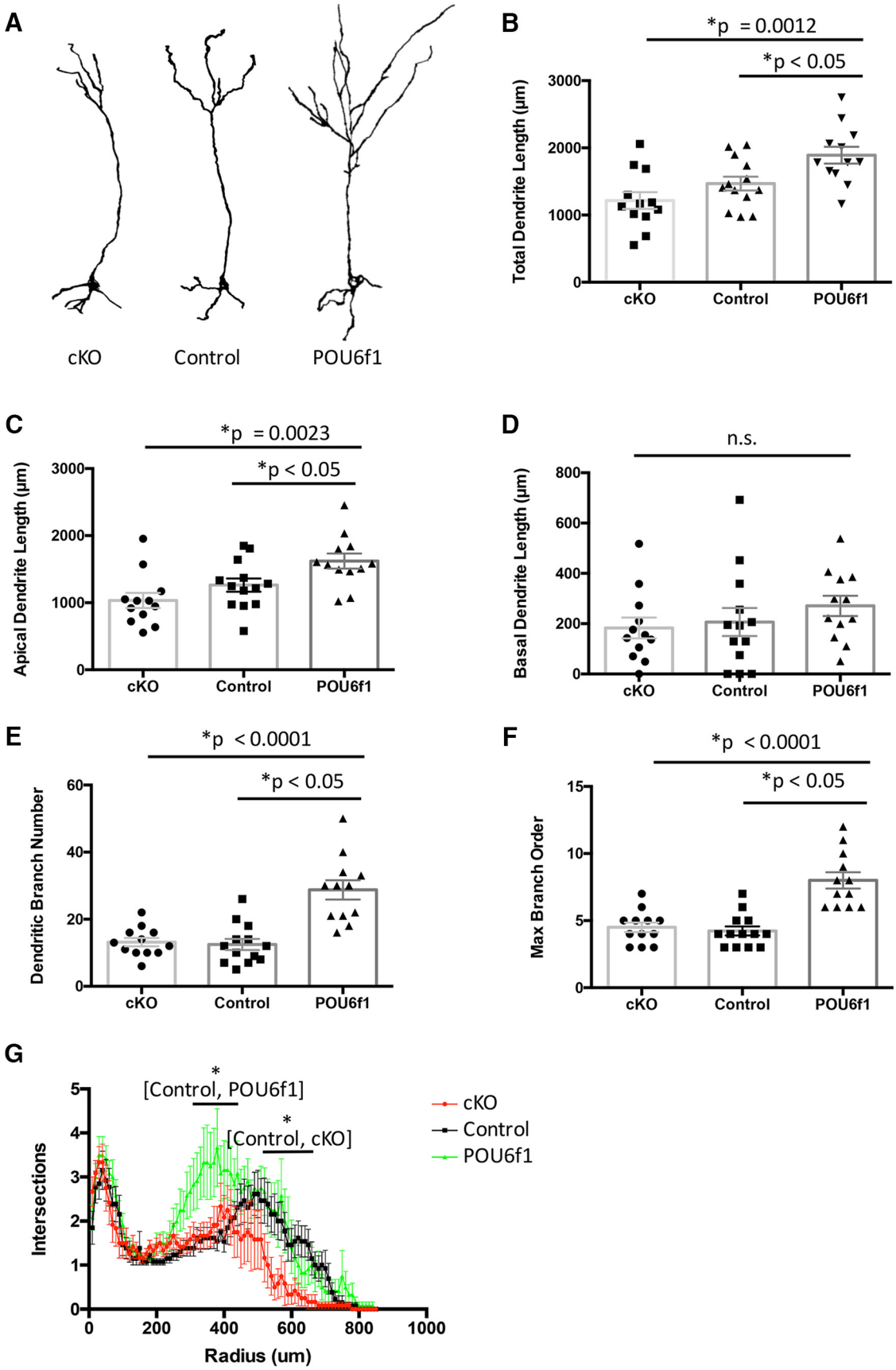

Figure 6. *POU6f1* influences morphological development of CRHR1 $^{+}$ neurons. ***A***, Representative reconstructions of GC morphology across experimental groups. ***B***, Comparisons of total dendrite length. cKO mean: 1216.7 $\pm$ 125 μm, control mean: 1469.5 $\pm$ 94 μm, *POU6f1* overexpression mean: 1891.2 $\pm$ 124.8 μm ($F_{(2,34)} = 8.254$, $p = 0.0012$, one-way ANOVA, posttest for linear trend, $R^2 = 0.3198$, $p = 0.0003$. $p < 0.05$ by *post hoc* Dunnett's multiple-comparisons test for the difference between control and *POU6f1* overexpression lengths; (*Figure legend continues.*)

membrane electrical capacitance (C_m) was observed between neurons that lacked *POU6f1* expression and controls (cKO mean: 13.41 ± 0.85 pF vs 13.03 ± 0.63 pF in controls; one-way ANOVA, $F_{(2,105)} = 6.236$, $p = 0.0028$, $p > 0.05$ *post hoc* Dunnett's multiple-comparisons test between cKO and control). Overexpression of *POU6f1*, however, resulted in higher C_m of CRHR1$^+$ GCs (Fig. 5*G*; 16.53 ± 0.83 pF in *POU6f1*-overexpressing cells vs 13.03 ± 0.63 pF in controls; $p < 0.05$, *post hoc* Dunnett's multiple-comparisons test between *POU6f1*-overexpressing cells and controls), with a significant linear trend identified for C_m dependent on levels of *POU6f1* ($R^2 = 0.06733$, $p = 0.0059$). This observation suggested a role for *POU6f1* in membrane outgrowth or branching of CRHR1$^+$ GCs.

POU6f1 influences dendritic branching in CRHR1$^+$ neurons

Having established that levels of *POU6f1* in CRHR1$^+$ cells are associated with a linear increase in C_m, we next examined the effects of *POU6f1* expression on dendritic outgrowth. Loss- and gain-of-function groups were again established using *CRHR1*-Cre mice to conditionally excise or overexpress *POU6f1* in CRHR1$^+$ cells, respectively. Cells were targeted with sparse viral labeling to enable single-cell analysis for the effects of *POU6f1* on morphological development of CRHR1$^+$ GCs. Using this approach, we observed increased total dendrite length associated with higher levels of *POU6f1* expression (Fig. 6*A*,*B*; 1469.5 ± 94 μm for controls vs 1891.2 ± 124.8 μm for overexpression; one-way ANOVA, $F_{(2,34)} = 8.254$, $p = 0.0012$, $p < 0.05$, Dunnett's multiple-comparisons test, $n = 3$ animals per group, $n = 12$–13 cells per group, means reported as means ± SE; posttest for linear trend $R^2 = 0.3198$, $p = 0.0003$). This increase in total dendritic length was primarily due to an increase in apical dendrite length (Fig. 6*C*; one-way ANOVA, $F_{(2,34)} = 7.280$, $p = 0.0023$, $p < 0.05$ Dunnett's multiple-comparisons test; 1620.3 ± 112.2 μm vs 1262.8 ± 90.4 μm for controls). Moreover, we again observed a linear association between the lengths of apical dendrites with respect to levels of *POU6f1* expression (posttest for linear trend, $R^2 = 0.2949$, $p = 0.0006$). This contrasted with unchanged lengths of basal dendrites for CRHR1$^+$ granule neurons regardless of *POU6f1* expression (Fig. 6*D*; cKO: 182.9 ± 41.4 μm, control: 206.7 ± 57.9 μm, POU6f1 overexpression: 270.9 ± 40.4 μm; one-way ANOVA, $F_{(2,34)} = 0.9214$, $p = 0.4077$). Increased apical dendrite lengths associated with increased *POU6f1* expression provided further support that *POU6f1* influences the functional development of dendrodendritic synapses with M/T cells because apical dendrites of mature GCs project into the EPL to establish such contacts (Shepherd et al., 2004; Schoppa, 2006).

To determine whether changes in apical dendrite length associated with *POU6f1* expression were also accompanied by changes in branch architecture, we measured both the total dendritic branch number and the maximum branch order for neurons in each group. We found that *POU6f1* overexpression in CRHR1$^+$ cells resulted in increased formation of dendritic branches (Fig. 6*E*; 12.46 ± 1.27 branches for control vs 28.75 ± 2.85 branches for *POU6f1* overexpression; one-way ANOVA, $F_{(2,34)} = 20.57$, $p < 0.0001$; *post hoc* Dunnett's multiple-comparisons test, $p < 0.05$ for control vs *POU6f1* overexpression). Moreover, the maximum branch order for neurons overexpressing *POU6f1* was greater than that of control (Fig. 6*F*; 8 ± 0.60 for POU6f1-overexpressing neurons vs 4.23 ± 0.26 for controls; one-way ANOVA, $F_{(2,34)} = 22.01$, $p < 0.0001$; *post hoc* Dunnett's multiple-comparisons test, $p < 0.05$ for control vs *POU6f1* overexpression). These results suggested that *POU6f1* influences dendritic branch formation and architecture in CRHR1$^+$ neurons. To examine the consequence of changed *POU6f1* expression on dendrite patterning, we further performed Sholl analysis (Fig. 6*G*) on traced dendritic branches. For this, we quantified branch intersections with concentric circles drawn starting from the somata of traced neurons, moving in 10 μm steps distally to cover the entirety of dendritic expanse. Both *POU6f1* cKO and *POU6f1*-overexpressing neurons showed changes in neuronal arborization compared with controls (two-way ANOVA, $F_{(2,2890)} = 68.72$, $p < 0.0001$ for levels of *POU6f1* as a source of variation). Loss of *POU6f1* expression resulted in reduced branching complexity relative to controls ($p < 0.05$, at radii of 520–650 μm distal to somas, Bonferroni multiple comparisons *post hoc* test), whereas *POU6f1* overexpression enhanced branching complexity ($p < 0.05$, at radii of 290–410 μm distal to somas). Together, the above results suggest that the *POU6f1* transcription program influences dendritic outgrowth and branch patterning in CRHR1$^+$ neurons.

Discussion

Plasticity in the adult brain is typified by activity-dependent structural alterations (Volkmar and Greenough, 1972; Magariños et al., 1996). The mouse OB circuit features ongoing, activity-dependent structural changes via integration of adult-born GCs. Interestingly, enhanced activity by odor enrichment or learning does not affect dendritic arborization of M/T cells (Mizrahi and Katz, 2003), the principal excitatory cells of the OB that relay multiple streams of output from the bulb (Fukunaga et al., 2012). The structural rigidity of M/T cells contrasts sharply with remodeling observed in newborn inhibitory neurons in the bulbs of animals subjected to odor task learning and enrichment (Saghatelyan et al., 2005; Arenkiel et al., 2011; Breton-Provencher et al., 2016; Huang et al., 2016; Quast et al., 2017). This suggests that, in the OB, activity-dependent circuit sculpting is primarily the domain of interneuron dynamics. However, the molecular pathways by which interneurons initiate and maintain structural changes in response to sensory input remain largely unresolved.

We recently discovered an interneuron-to-interneuron signaling mechanism mediated via activity-dependent, locally secreted CRH in the bulb. This neuropeptidergic signaling cascade influences morphology and functional maturation of CRHR1$^+$ GCs (Garcia et al., 2014). Both CRH (Swanson et al., 1983) and its main CNS receptor CRHR1 (Chalmers et al., 1995) are expressed in other brain areas and the local release of CRH in these areas is

←

(*Figure legend continued.*) $n = 3$ animals per group, $n = 12$–13 cells per group). ***C***, Quantifications of apical dendrite length. cKO mean: 1033.7 ± 113.5 μm, control mean: 1262.8 ± 90.4 μm, *POU6f1* overexpression mean: 1620.3 ± 112.2 μm. ($p = 0.0023$, one-way ANOVA, Dunnett's multiple-comparisons test $p < 0.05$ for difference between control and gain-of-function groups; posttest for linear trend, $R^2 = 0.2949$, $p = 0.0006$.) ***D***, Basal dendrite lengths. cKO mean: 182.9 ± 41.4 μm, control mean: 206.7 ± 57.9 μm, *POU6f1* overexpression mean: 270.9 ± 40.4 μm. ($F_{(2,34)} = 0.9214$, $p = 0.4077$, one-way ANOVA.) ***E***, Comparisons of dendrite branch number. cKO mean: 13.2 ± 1.25 branches, control mean: 12.46 ± 1.27 branches, *POU6f1* overexpression mean: 28.75 ± 2.85 branches ($F_{(2,34)} = 20.57$, $p < 0.0001$, one-way ANOVA; $p < 0.05$ by *post hoc* Dunnett's multiple-comparisons test for control versus *POU6f1* overexpression). ***F***, Comparisons of maximum branch order. cKO mean: 4.5 ± 0.36, control mean: 4.23 ± 0.26, *POU6f1* overexpression mean: 8 ± 0.60. ($F_{(2,34)} = 22.01$, $p < 0.0001$, one-way ANOVA; $p < 0.05$ by *post hoc* Dunnett's multiple-comparisons test for control versus *POU6f1* overexpression). ***G***, Sholl analysis of the number of branch intersections with concentrically drawn circles at consecutive 10 μM increments distally from the soma ($F_{(2,2890)} = 68.72$, $p < 0.0001$ for levels of *POU6f1* as source of variation, two-way ANOVA; $p < 0.05$ for differences between cKO and control groups at radii of 520–650 μM; $p < 0.05$ for differences between control and *POU6f1* overexpression groups at radii of 290–410 μM). All data are reported as mean ± SE.

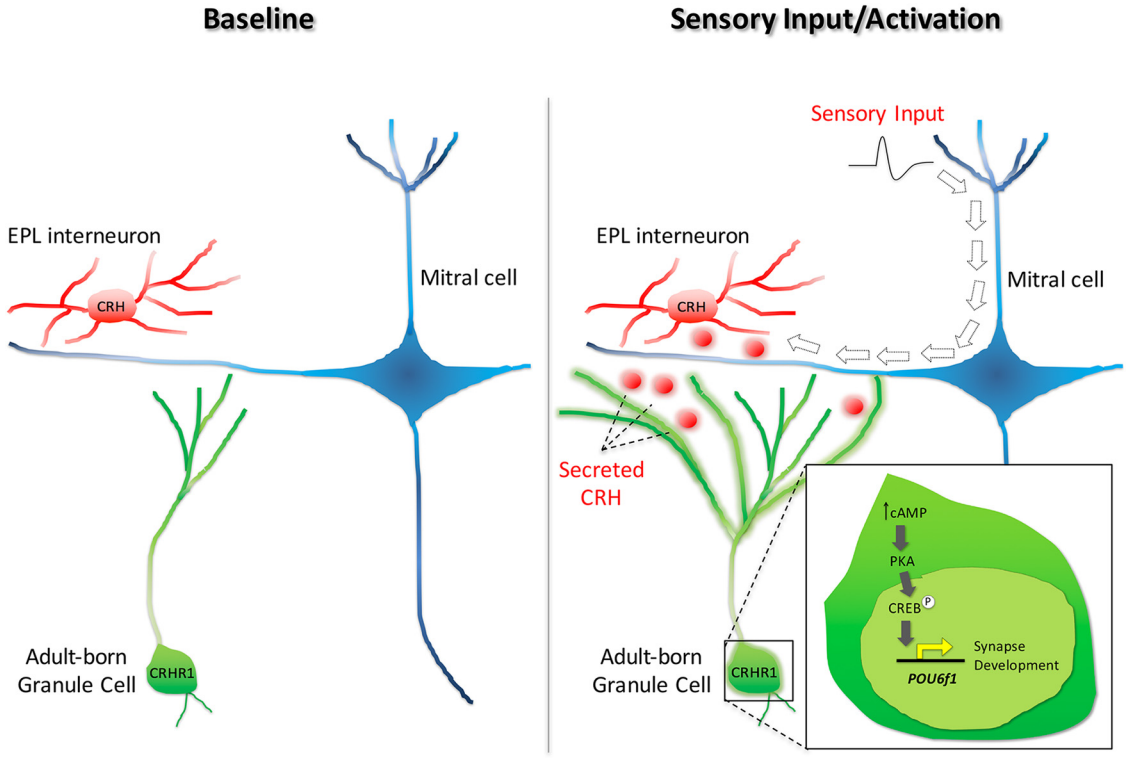

Figure 7. *POU6f1* regulates synapse and dendrite plasticity in CRHR1$^+$ GCs of the OB. Proposed model: Sensory input and experience induce release of CRH from local interneurons of the EPL of the bulb. Secreted CRH binds to CRHR1 expressed by adult-born granule interneurons, which in turn activates *POU6f1* transcription within GCs. The *POU6f1* transcription program elaborates GC dendrites and promotes dendrodendritic synapse formation with excitatory mitral cells of the bulb. This activity-dependent peptide signaling mechanism reshapes bulb circuitry and thus output to higher brain areas for sensory processing.

also influenced by environmental cues (Imaki et al., 1991). Therefore, we hypothesize that CRH and/or other neuropeptide signaling networks are broadly embedded to convey network-shaping effects of sensory activity. Indeed, others have reported that CRH signaling within the hippocampus remodels pyramidal cell dendrites in response to stress (Chen et al., 2004). The role of CRH in activity-dependent circuit restructuring in the bulb may therefore exemplify a more generalizable principle of peptide-mediated plasticity.

Here, we examined a mechanism by which local CRH signaling reshapes circuitry in the adult OB. We found that CRHR1 activity influences expression of the transcription factor *POU6f1* in neural cells and that expression of this factor is required for normal synaptic integration and dendritic elaboration.

Local CRH signaling promotes activation of the transcriptional regulator POU6f1

CRH-to-CRHR1 signaling has been implicated previously in altered dendritic morphology in the hippocampus (Chen et al., 2004) and bulk-loaded CRH is reported to induce expression of immediate early genes such as the transcription factor *c-fos* in other brain regions (Clark et al., 1991; Parkes et al., 1993). However, to date, no link between local CRH signaling and a specific transcriptional program that regulates dendritic plasticity has been established. Here, we performed a screen for gene expression changes downstream of CRH signaling in the bulb and found that CRHR1 activation was associated with expression of the transcription factor *POU6f1*. Our screen was performed on whole bulb tissue and thus did not discern cell-type specificity of expression changes. However, *in situ* hybridization against *POU6f1* in the OBs of adult *CRHR1*$^{-/-}$ mice showed that *CRHR1*$^{-/-}$ cells in the GCL downregulated expression of *POU6f1*.

In vitro data further suggest that *POU6f1* is modulated directly by CREB-dependent transcription in response to CRHR1 activity. This is consistent with the known CREB-activating mechanism of CRHR1, a G_S-protein-coupled receptor (Berger et al., 2006; Blank et al., 2003). However, it is possible that an alternative or additional CREB-dependent mechanism of *POU6f1* activation operates *in vivo*. Bulleit et al., 1994 showed that *POU6f1* mRNA increased in cultured neurons after NMDA receptor activation. NMDAR-mediated calcium influx could therefore also contribute to CREB-dependent transcriptional activation (Sheng et al., 1990) of *POU6f1 in vivo*.

POU6f1 expression correlates with neuronal maturity

We found that *POU6f1*::HA is expressed progressively as adult-born neurons develop. Moreover, most mature (NeuN$^+$) GCs also expressed *POU6f1*::HA, and reciprocally most *POU6f1*::HA$^+$ GCs expressed NeuN, suggesting that *POU6f1* expression correlates with maturation of GCs. Interestingly, NeuN expression, which appears after developing neurons exit the cell cycle (Kim et al., 2009), reportedly increases rapidly in adult-born neurons of the OB during the first 2 weeks after birth before plateauing (Petreanu and Alvarez-Buylla, 2002). Therefore, NeuN is predicted to appear before expression of both *CRHR1* (Garcia et al., 2014) and *POU6f1*::HA. We found previously that *CRHR1* expression was required for normal rates of survival (Garcia et al., 2014) and report here that *POU6f1* influences both structural and functional aspects of development in *CRHR1*-expressing cells. Therefore, early NeuN expression relative to expression of either *CRHR1* or *POU6f1* in adult-born neurons suggests that they may

be marked for generalized maturation (i.e., cell cycle exit) before subsequent expression of genes involved in neuropeptide signaling. Interestingly, we did not observe a direct effect of *POU6f1* on survival of CRHR1$^+$ adult-born (data not shown). This is consistent with the notion that *POU6f1* influences later aspects of maturation.

POU6f1 mediates synapse and dendrite branch formation

We found that loss of *POU6f1* reduced the quantal content, encompassing the number of release sites and/or probability of vesicle release, of excitatory synaptic connections formed onto CRHR1$^+$ GCs. Increased *POU6f1* expression resulted in delayed excitatory current kinetics in a manner consistent with increased input by dendrodendritic synapses with M/T cells. This was further consistent with analysis suggesting that *POU6f1* promotes formation of apical dendrites, onto which dendrodendritic synapses between CRHR1$^+$ GCs and M/T form. Together, these results indicate that *POU6f1* contributes to the content and function of excitatory synaptic inputs onto CRHR1$^+$ cells.

We observed that low levels of *POU6f1* were associated with reduced total dendrite length in GCs and high levels of *POU6f1* resulted in increased dendrite length. Interestingly, these differences were almost entirely explained by changes in apical dendrite lengths because basal dendrites were unaffected by *POU6f1* expression. This has intriguing implications for whether *POU6f1* influences preferentially dendrodendritic synapses of GCs with M/T cells, which tend to make contacts onto distal apical dendrites of GCs (Schoppa, 2006), over inputs by centrifugal fibers, which tend to form basal and proximal connections onto GCs (Shipley and Adamek, 1984; Laaris et al., 2007). It is tempting to speculate that local CRH secreted from within the EPL promotes the formation of dendrodendritic synapses in this same layer to enhance olfaction at proximal sites of sensory processing. Others have reported that functionally correlated GCs appear to cluster (Wienisch and Murthy, 2016) in alignment with M/T cells and along the borders of odor-specific glomeruli (Guthrie et al., 1993; Wilhite et al., 2006). A localized peptidergic cue that is secreted with odor activity to guide synapse formation in such a functional vicinity provides a potential mechanism by which these topographic relationships are established and/or maintained across the surface of the bulb. However, more direct testing would be required to investigate such a possibility.

The notion that *POU6f1* reshapes GC connectivity was further supported by observations of increased dendritic branch number, maximum branch order, and branch pattern complexity in *POU6f1*-overexpressing neurons. Such intricate outgrowths of GC arborizations could give rise to more and/or varied granule-to-M/T cell contacts, which tend to form on lateral secondary dendrites of M/T cells distal to their somas (Bartel et al., 2015). Functionally, more numerous or expanded GC connections may contribute to broadened GC tuning and contrast enhancement (Cazakoff et al., 2014) or serve as a means to synchronize M/T firing, such that the bulb relays a tight representation of the collective attributes of complex odors (Davison and Katz, 2007). Such outcomes would be promising paths for future inquiry.

One caveat to our studies arises from the expression pattern of *CRHR1* in adult-born neurons, thus affecting our maniuplations in *CRHR1*-Cre mice. *CRHR1* is expressed by adult-born neurons both during and continually after integration, when dendrite extension has ceased (Mizrahi, 2007). Our assays examined aspects of plasticity normally restricted to the preintegration period. Therefore, because our experiments targeted both younger and older CRHR1$^+$ GCs, our interpretations likely underestimate the effects of *POU6f1* in shaping these processes in younger cells. This may explain why we observed no differences in odor learning or short-term olfactory behavior in cKO versus control mice (data not shown). More selective tests of developmental contributions of *POU6f1* would require a *CRHR1*-Cre inducible mouse model.

Nevertheless, our data suggest that, within CRHR1$^+$ GCs in the adult OB, *POU6f1* is a transcriptional regulator that can influence dendrite specification and is required to establish a normal complement of excitatory synapses onto CRHR1$^+$ GCs. The effects of loss and gain of *POU6f1* in the present studies did not perfectly mirror the effects of loss and gain of *CRHR1* in our previous studies (Garcia et al., 2014). This implies that CRH signaling in the OB likely results in other changes beyond those mediated by *POU6f1* and that *POU6f1* may have roles outside of conveying the effects of local CRH signaling. However, the data herein present the first evidence that a specific transcription program can be initiated downstream of activity-dependent local peptide signaling to the end effect of functional circuit refinement in the adult brain (Fig. 7).

Note Added in Proof: The tenth author's last name was accidentally misspelled on the Early Release version published January 5, 2018. The name has now been corrected.

References

Aguilera G, Harwood J, Wilson J, Morell J, Brown JH, Catt KJ (1983) Mechanisms of action of corticotropin releasing factor and other regulators of corticotropin release in rat pituitary cells. J Biol Chem 258:8039–8045. Medline

Alonso M, Viollet C, Gabellec MM, Meas-Yedid V, Olivo-Marin JC, Lledo PM (2006) Olfactory discrimination learning increases the survival of adult-born neurons in the olfactory bulb. J Neurosci 26:10508–10513. CrossRef Medline

Alvarez-Buylla A, Temple S (1998) Stem cells in the developing and adult nervous system. J Neurobiol 36:105–110. CrossRef Medline

Andersen B, Schonemann MD, Pearse RV 2nd, Jenne K, Sugarman J, Rosenfeld MG (1993) Brn-5 is a divergent POU domain factor highly expressed in layer IV of the neocortex. J Biol Chem 268:23390–23398. Medline

Arenkiel BR, Hasegawa H, Yi JJ, Larsen RS, Wallace ML, Philpot BD, Wang F, Ehlers MD (2011) Activity-induced remodeling of olfactory bulb microcircuits revealed by monosynaptic tracing. PLoS One 6:e29423. CrossRef Medline

Atasoy D, Aponte Y, Su HH, Sternson SM (2008) A FLEX switch targets Channelrhodopsin-2 to multiple cell types for imaging and long-range circuit mapping. J Neurosci 28:7025–7030. CrossRef Medline

Bartel DL, Rela L, Hsieh L, Greer CA (2015) Dendrodendritic synapses in the mouse olfactory bulb external plexiform layer. J Comp Neurol 523:1145–1161. CrossRef Medline

Bassett AR, Tibbit C, Ponting CP, Liu JL (2013) Highly efficient targeted mutagenesis of *Drosophila* with the CRISPR/Cas9 system. Cell Rep 4:220–228. CrossRef Medline

Berger H, Heinrich N, Wietfeld D, Bienert M, Beyermann M (2006) Evidence that corticotropin-releasing factor receptor type 1 couples to Gs and Gi-proteins through different conformations of its J-domain. Br J Pharmacol 149:942–947. Medline

Blank T, Nijholt I, Grammatopoulos DK, Randeva HS, Hillhouse EW, Spiess J (2003) Corticotropin-releasing factor receptors couple to multiple G-proteins to activate diverse intracellular signaling pathways in mouse hippocampus: role in neuronal excitability and associative learning. J Neurosci 23:700–707. Medline

Breton-Provencher V, Bakhshetyan K, Hardy D, Bammann RR, Cavarretta F, Snapyan M, Côté D, Migliore M, Saghatelyan A (2016) Principal cell activity induces spine relocation of adult-born interneurons in the olfactory bulb. Nat Commun 7:12659. CrossRef Medline

Bulleit RF, Cui H, Wang J, Lin X (1994) NMDA receptor activation in differentiating cerebellar cell cultures regulates the expression of a new POU gene, Cns-1. J Neurosci 14:1584–1595. Medline

Carleton A, Petreanu LT, Lansford R, Alvarez-Buylla A, Lledo PM (2003) Becoming a new neuron in the adult olfactory bulb. Nat Neurosci 6:507–518. CrossRef Medline

Carson JP, Eichele G, Chiu W (2005) A method for automated detection of gene expression required for the establishment of a digital transcriptome-wide gene expression atlas. J Microsc 217:275–281. CrossRef Medline

Cauthron JL, Stripling JS (2014) Long-term plasticity in the regulation of olfactory bulb activity by centrifugal fibers from piriform cortex. J Neurosci 34:9677–9687. CrossRef Medline

Cazakoff BN, Lau BY, Crump KL, Demmer HS, Shea SD (2014) Broadly tuned and respiration-independent inhibition in the olfactory bulb of awake mice. Nat Neurosci 17:569–576. CrossRef Medline

Chalmers DT, Lovenberg TW, De Souza EB (1995) Localization of novel corticotropin-releasing factor receptor (CRF2) mRNA expression to specific subcortical nuclei in rat brain: comparison with CRF1 receptor mRNA expression. J Neurosci 15:6340–6350. Medline

Chen Y, Bender RA, Brunson KL, Pomper JK, Grigoriadis DE, Wurst W, Baram TZ (2004) Modulation of dendritic differentiation by corticotropin-releasing factor in the developing hippocampus. Proc Natl Acad Sci U S A 101:15782–15787. CrossRef Medline

Clark M, Weiss SR, Post RM (1991) Expression of c-fos mRNA in rat brain after intracerebroventricular administration of corticotropin-releasing hormone. Neurosci Lett 132:235–238. CrossRef Medline

Cong L, Ran FA, Cox D, Lin S, Barretto R, Habib N, Hsu PD, Wu X, Jiang W, Marraffini LA, Zhang F (2013) Multiplex genome engineering using CRISPR/Cas systems. Science 339:819–823. CrossRef Medline

Corotto FS, Henegar JR, Maruniak JA (1994) Odor deprivation leads to reduced neurogenesis and reduced neuronal survival in the olfactory bulb of the adult mouse. Neuroscience 61:739–744. CrossRef Medline

Cui H, Bulleit RF (1998) Expression of the POU transcription factor Brn-5 is an early event in the terminal differentiation of CNS neurons. J Neurosci Res 52:625–632. CrossRef Medline

Cummings DM, Henning HE, Brunjes PC (1997) Olfactory bulb recovery after early sensory deprivation. J Neurosci 17:7433–7440. Medline

Davison IG, Katz LC (2007) Sparse and selective odor coding by M/T neurons in the main olfactory bulb. J Neurosci 27:2091–2101. CrossRef Medline

Edgar R, Domrachev M, Lash AE (2002) Gene Expression Omnibus: NCBI gene expression and hybridization array data repository. Nucleic Acids Res 30:207–210. CrossRef Medline

Fiske BK, Brunjes PC (2001) Cell death in the developing and sensory-deprived rat olfactory bulb. J Comp Neurol 431:311–319. CrossRef Medline

Fukunaga I, Berning M, Kollo M, Schmaltz A, Schaefer AT (2012) Two distinct channels of olfactory bulb output. Neuron 75:320–329. CrossRef Medline

Gao Y, Strowbridge BW (2009) Long-term plasticity of excitatory inputs to granule cells in the rat olfactory bulb. Nat Neurosci 12:731–733. CrossRef Medline

Garcia I, Quast KB, Huang L, Herman AM, Selever J, Deussing JM, Justice NJ, Arenkiel BR (2014) Local CRH signaling promotes synaptogenesis and circuit integration of adult-born neurons. Dev Cell 30:645–659. CrossRef Medline

Giguère V, Labrie F, Côté J, Coy DH, Sueiras-Diaz J, Schally AV (198s) Stimulation of cAMP accumulation and corticotropin releasing factor in rat anterior cells: site of glucocorticoid action. Proc Natl Acad Sci U S A 79:3466–3469. Medline

Gonzalez GA, Montminy MR (1989) Cyclic AMP stimulates somatostatin gene transcription by phosphorylation of CREB at serine 133. Cell 59: 675–680. CrossRef Medline

Guthrie KM, Anderson AJ, Leon M, Gall C (1993) Odor-induced increases in c-fos mRNA expression reveal an anatomical "unit" for odor processing in olfactory bulb. Proc Natl Acad Sci U S A 90:3329–3333. Medline

Huang L, Garcia I, Jen H, Arenkiel BR (2013) Reciprocal connectivity between mitral cells and external plexiform layer interneurons in the mouse olfactory bulb. Front Neural Circuits 7:32. CrossRef Medline

Huang L, Ung K, Garcia I, Quast KB, Cordiner K, Saggau P, Arenkiel BR (2016) Task learning promotes plasticity of interneuron connectivity maps in the olfactory bulb. J Neurosci 36:8856–8871. CrossRef Medline

Imaki T, Nahan JL, Rivier C, Sawchenko PE, Vale W (1991) Differential regulation of corticotropin-releasing factor mRNA in rat brain regions by glucocorticoids and stress. J Neurosci 11:585–599. Medline

Imayoshi I, Sakamoto M, Ohtsuka T, Takao K, Miyakawa T, Yamaguchi M, Mori K, Ikeda T, Itohara S, Kageyama R (2008) Roles of continuous neurogenesis in the structural and functional integrity of the adult forebrain. Nat Neurosci 11:1153–1161. CrossRef Medline

Isaacson JS, Strowbridge BW (1998) Olfactory reciprocal synapses: dendritic signaling in the CNS. Neuron 20:749–761. CrossRef Medline

Jahr CE, Nicoll RA (1980) Dendrodendritic inhibition: demonstration with intracellular recording. Science 207:1473–1475. CrossRef Medline

Justice NJ, Yuan ZF, Sawchenko PE, Vale W (2008) Type 1 corticotropin-releasing factor receptor expression reported in BAC transgenic mice: implications for reconciling ligand-receptor mismatch in the central corticotropin-releasing factor system. J Comp Neurol 511:479–496. CrossRef Medline

Kato HK, Gillet SN, Peters AJ, Isaacson JS, Komiyama T (2013) Parvalbumin-expressing interneurons linearly control olfactory bulb output. Neuron 80:1218–1231. CrossRef Medline

Kelsch W, Lin CW, Mosley CP, Lois C (2009) A critical period for activity-dependent synaptic development during olfactory bulb adult neurogenesis. J Neurosci 29:11852–11858. CrossRef Medline

Kent W (2002) BLAT: the BLAST-like alignment tool. Genome Res 12:656–664. CrossRef Medline

Kim KK, Adelstein RS, Kawamoto S (2009) Identification of neuronal nuclei (NeuN) as Fox-3, a new member of the Fox-1 gene family of splicing factors. J Biol Chem 284:31052–31061. CrossRef Medline

Laaris N, Puche A, Ennis M (2007) Complementary postsynaptic activity patterns elicited in olfactory bulb by stimulation of mitral/tufted and centrifugal fiber inputs to granule cells. J Neurophysiol 97:296–306. CrossRef Medline

Latchman DS (1999) POU family transcription factors in the nervous system. J Cell Physiol 179:126–133. CrossRef Medline

Lein E, et al. (2007) Genome-wide atlas of gene expression in the adult mouse brain. Nature 445:168–176. CrossRef Medline

Lemasson M, Saghatelyan A, Olivo-Marin JC, Lledo PM (2005) Neonatal and adult neurogenesis provide two distinct populations of newborn neurons to the mouse olfactory bulb. J Neurosci 25:6816–6825. CrossRef Medline

Luskin MB (1993) Restricted proliferation and migration of postnatally generated neurons derived from the forebrain subventricular zone. Neuron 11:173–189. CrossRef Medline

Magariños AM, McEwen BS, Flügge G, Fuchs E (1996) Chronic psychosocial stress causes apical dendritic atrophy of hippocampal CA3 pyramidal neurons in subordinate tree shrews. J Neurosci 16:3534–3540. Medline

Mandairon N, Sacquet J, Garcia S, Ravel N, Jourdan F, Didier A (2006) Neurogenic correlates of an olfactory discrimination task in the adult olfactory bulb. Eur J Neurosci 24:3578–3588. CrossRef Medline

Ming GL, Song H (2005) Adult neurogenesis in the mammalian central nervous system. Annu Rev Neurosci 28:223–250. CrossRef Medline

Miyamichi K, Shlomai-Fuchs Y, Shu M, Weissbourd BC, Luo L, Mizrahi A (2013) Dissecting local circuits: parvalbumin interneurons underlie broad feedback control of olfactory bulb output. Neuron 80:1232–1245. CrossRef Medline

Mizrahi A (2007) Dendritic development and plasticity of adult-born neurons in the mouse olfactory bulb. Nat Neurosci 10:444–452. CrossRef Medline

Mizrahi A, Katz LC (2003) Dendritic stability in the adult olfactory bulb. Nat Neurosci 6:1201–1207. CrossRef Medline

Montminy MR, Sevarino KA, Wagner JA, Mandel G, Goodman RH (1986) Identification of a cyclic-AMP-responsive element within the rat somatostatin gene. Proc Natl Acad Sci U S A 83:6682–6686. CrossRef Medline

Monuki ES, Weinmaster G, Kuhn R, Lemke G (1989) SCIP: a glial POU domain gene regulated by cyclic AMP. Neuron 3:783–793. CrossRef Medline

Mouret A, Gheusi G, Gabellec MM, de Chaumont F, Olivo-Marin JC, Lledo PM (2008) Learning and survival of newly generated neurons: when time matters. J Neurosci 28:11511–11516. CrossRef Medline

Mullen RJ, Buck CR, Smith AM (1992) NeuN, a neuronal specific nuclear protein in vertebrates. Development 116:201–211. Medline

Najbauer J, Leon M (1995) Olfactory experience modulated apoptosis in the developing olfactory bulb. Brain Res 674:245–251. CrossRef Medline

Nielsen SM, Nielsen LZ, Hjorth SA, Perrin MH, Vale WW (2000) Constitutive activation of tethered-peptide/corticotropin-releasing factor receptor chimeras. Proc Natl Acad Sci U S A 97:10277–10281. CrossRef Medline

Okamoto K, Wakamiya M, Noji S, Koyama E, Taniguchi S, Takemura R,

Copeland NG, Gilbert DJ, Jenkins NA, Muramatsu M (1993) A novel class of murine POU gene predominantly expressed in central nervous system. J Biol Chem 268:7449–7457. Medline

Orona E, Scott JW, Rainer EC (1983) Different granule cell populations innervate superficial and deep regions of the external plexiform layer in rat olfactory bulb. J Comp Neurol 217:227–237. CrossRef Medline

Orona E, Rainer EC, Scott JW (1984) Dendritic and axonal organization of mitral and tufted cells in the rat olfactory bulb. J Comp Neurol 226:346–356. CrossRef Medline

Parkes D, Rivest S, Lee S, Rivier C, Vale W (1993) Corticotropin-releasing factor activates c-fos, NGFI-B, and corticotropin-releasing factor gene expression within the paraventricular nucleus of the rat hypothalamus. Mol Endocrinol 7:1357–1367. CrossRef Medline

Petreanu L, Alvarez-Buylla A (2002) Maturation and death of adult-born olfactory bulb granule neurons: role of olfaction. J Neurosci 22:6106–6113. Medline

Quast KB, Ung K, Froudarakis E, Huang L, Herman I, Addison AP, Ortiz-Guzman J, Cordiner K, Saggau P, Tolias AS, Arenkiel BR (2017) Developmental broadening of inhibitory sensory maps. Nat Neurosci 20:189–199. CrossRef Medline

Saghatelyan A, Roux P, Migliore M, Rochefort C, Desmaisons D, Charneau P, Shepherd GM, Lledo PM (2005) Activity-dependent adjustments of the inhibitory network in the olfactory bulb following early postnatal deprivation. Neuron 46:103–116. CrossRef Medline

Schoppa NE (2006) AMPA/kainate receptors drive rapid output and precise synchrony in olfactory bulb granule cells. J Neurosci 26:12996–13006. CrossRef Medline

Sheng M, McFadden G, Greenberg ME (1990) Membrane depolarization and calcium induce c-fos transcription via phosphorylation of transcription factor CREB. Neuron 4:571–582. CrossRef Medline

Shepherd GM, Chen WR, Greer CA, eds (2004) Olfactory bulb, Ed 5. Oxford: Oxford UP.

Shipley MT, Adamek GD (1984) The connections of the mouse olfactory bulb: a study using orthograde and retrograde transport of wheat germ agglutinin conjugated to horseradish peroxidase. Brain Res Bull 12:669–688. CrossRef Medline

Smith GW, Aubry JM, Dellu F, Contarino A, Bilezikjian LM, Gold LH, Chen R, Marchuk Y, Hauser C, Bentley CA, Sawchenko PE, Koob GF, Vale W, Lee KF (1998) Corticotropin releasing factor receptor 1-deficient mice display decreased anxiety, impaired stress response, and aberrant neuroendocrine development. Neuron 20:1093–1102. CrossRef Medline

Soule HD, Vazguez J, Long A, Albert S, Brennan M (1973) A human cell line from a pleural effusion derived from a breast carcinoma. J Nat Cancer Inst 51:1409–1416. CrossRef Medline

Storey JD, Tibshirani R (2003) Statistical significance for genomewide studies. Proc Natl Acad Sci U S A 100:9440–9445. CrossRef Medline

Swanson LW, Sawchenko PE, Rivier J, Vale WW (1983) Organization of ovine corticotropin-releasing factor immunoreactive cells and fibers in the rat brain: an immunohistochemical study. Neuroendocrinology 36:165–186. CrossRef Medline

Thiel G, Cibelli G (1999) Corticotropin-releasing factor and vasoactive intestinal polypeptide activate gene transcription through the cAMP signaling pathway in a catecholaminergic immortalized neuron. Neurochem Int 34:183–191. CrossRef Medline

Uhlén M, et al. (2015) Proteomics: tissue-based map of the human proteome. Science 347:1260419. CrossRef Medline

Volkmar FR, Greenough WT (1972) Rearing complexity affects branching of dendrites in the visual cortex of the rat. Science 176:1445–1447. CrossRef Medline

Wang P, Wang Q, Sun J, Wu J, Li H, Zhang N, Huang Y, Su B, Li RK, Liu L, Zhang Y, Elsholtz HP, Hu J, Gaisano HY, Jin T (2009) POU homeodomain protein Oct-1 functions as a sensor for cyclic AMP. J Biol Chem 284:26456–26465. CrossRef Medline

Wey E, Lyons GE, Schäfer BW (1994) A human POU domain gene, mPOU, is expressed in developing brain and specific adult tissues. Eur J Biochem 220:753–762. CrossRef Medline

Wienisch M, Murthy VN (2016) Population imaging at subcellular resolution supports specific and local inhibition by granule cells in the olfactory bulb. Sci Rep 6:29308. CrossRef Medline

Willhite DC, Nguyen KT, Masurkar AV, Greer CA, Shepherd GM, Chen WR (2006) Viral tracing identifies distributed columnar organization in the olfactory bulb. Proc Natl Acad Sci U S A 103:12592–12597. CrossRef Medline

Yamaguchi M, Mori K (2005) Critical period for sensory experience-dependent survival of newly generated granule cells in the adult mouse olfactory bulb. Proc Natl Acad Sci U S A 102:9697–9702. CrossRef Medline

Yaylaoglu MB, Titmus A, Visel A, Alvarez-Bolado G, Thaller C, Eichele G (2005) Comprehensive expression atlas of fibroblast growth factors and their receptors generated by a novel robotic in situ hybridization platform. Dev Dyn 234:371–386. CrossRef Medline

Yoshihara S, Takahashi H, Nishimura N, Naritsuka H, Shirao T, Hirai H, Yoshihara Y, Mori K, Stern PL, Tsuboi A (2012) 5T4 glycoprotein regulates the sensory input-dependent development of a specific subtype of newborn interneurons in the mouse olfactory bulb. J Neurosci 32:2217–2226. CrossRef Medline

Zerbino DR, Wilder SP, Johnson N, Juettemann T, Flicek PR (2015) The Ensembl regulatory build. Genome Biol 16:56. CrossRef Medline

Zhao C, Deng W, Gage FH (2008) Mechanisms and functional implications of adult neurogenesis. Cell 132:645–660. CrossRef Medline